conducted following protocols approved by the Animal Care and Use Committee at Juntendo University.

Antibodies

To determine the epitope of the newly developed mouse anti-human CD26 mAbs, murine anti-human CD26 mAbs (clone 4G8, 1F7, 14D10, 5F8, 16D4B or 9C11) which have been already developed in our laboratory were used [18]. We have previously shown that these mAbs are divided into 5 separate groups by their epitopes, 4G8 recognizing the 1-247th AAs region of CD26, 1F7 and 14D10 recognizing the 248-358th AAs region of CD26, 5F8 recognizing the 359-449th (closer to the 359th) AAs region of CD26, 16D4B recognizing the 450-577th AAs region of CD26, and 9C11 recognizing the 359-653th (but different from 5F8 or 16D4B) AAs region of CD26. The humanized anti-CD26 mAb (YS110) was generated by utilizing the complementarity determining regions of the murine anti-human CD26 mAb 14D10 [18], and generously provided by Y's Therapeutics (Tokyo, Japan). To compare the staining pattern and intensity of human CD26 on formalin-fixed tissue sections, we used two commercial anti-human CD26 Abs available for CD26 detection by immunohistochemistry. One is the culture supernatant form of a mouse anti-human CD26 mAb (clone 44–4) purchased from MBL (Nagoya, Japan), and the other is a purified goat anti-human CD26 pAb purchased from R&D Systems (Minneapolis, MN). Human polyclonal IgG (venilon-I) was purchased from Alfresa Corporation (Tokyo, Japan), and mouse IgG_1 isotype control (clone MG1-45) was purchased from BioLegend (San Diego, CA). YS110, control human IgG, 4G8, 1F7, 5F8, 16D4B, 9C11, purified clone 18, clone 19, and mouse IgG_1 isotype control were labeled using an Alexa Fluor 647 Monoclonal Antibody Labeling Kit (Molecular Probes, Eugene, OR) according to the manufacturer's instructions.

cDNA constructs and transfection

As described previously [18], C-terminal deletion mutants of human CD26 cDNA constructs were generated by using Nco I restriction enzyme sites to delete domain representing the 740-766th AAs in the C terminus, using Nhe I to delete from the 578th AA, using BspE I to delete from the 450th AA, using Stu I to delete from the 359th AA, and using Pst I to delete from the 248th AA. These cDNAs were ligated in-frame into pcDL-SRα expression vector [20]. The green fluorescence protein (GFP)-expressing vector pEB6-CAG-GFP was a kind gift from Dr. Yoshihiro Miwa (Tsukuba University, Tsukuba, Japan) [21]. Each CD26 deletion construct in pcDL-SRα was co-transfected with pEB6-CAG-GFP into COS-7 cells using Lipofectamine 2000 reagent (Invitrogen, Carlsbad, CA). After 24 hours of transfection, cells were harvested, followed by staining with Alexa Fluor 647-labeled 4G8, 1F7, 5F8, YS110, clone 18 or clone 19, and then analyzed by flow cytometry.

Preparation of immunogen

Soluble CD26 (sCD26) was produced according to the method described previously [22]. Briefly, the expression vector RcSRα-26d3-9, which contains a deletion of the coding sequence for amino acids 3–9 of CD26, was transfected into a dihydrofolate reductase deficit Chinese hamster ovary (CHO) cell line, DXB-11 by electroporation, together with pMT-2 providing the dihydrofolate reductase gene. The transfected CHO cells were cultured in serum-free CHO-S-SFM II medium (Invitrogen) supplemented with 1 μM methotrexate (Nacalai Tesque, Kyoto, Japan). The culture supernatant was collected and subjected to affinity chromatography on ADA-Sepharose according to the method described previously [23]. Purified sCD26 was denatured in 8 M urea buffer supplemented with 20 mM HEPES and 50 mM dithiothreitol (DTT) by gentle rotation for 8 hours at RT.

Development of hybridomas and monoclonal anti-human CD26 antibodies

Denatured sCD26 was dialyzed in PBS, and 100 μg of protein per 50 μl of PBS was emulsified with 50 μl of adjuvant, TiterMax Gold (TiterMax USA, Norcross, GA). A 6-wk-old female BALB/c mouse was immunized s.c. with 100 μl of the emulsion seven times every two weeks and finally injected i.v. with half volume of the emulsion. Three days after the final immunization, the spleen was removed and 100×10^6 spleen cells were fused with 100×10^6 P3U1 myeloma cells by using polyethylene glycol 4000 (Merck, Darmstadt, Germany) and were cultured in RPMI1640 supplemented with 10% fetal bovine serum (FBS, Japan Bioserum, Fukuyama, Japan), 5% BriClone (NICB, Dublin, Ireland) and HAT (Invitrogen) in 96-well flat-bottom plates (Costar, Corning Incorporated, Corning, NY). Hybridoma supernatants were screened for selective reactivity with human CD26 by using flow cytometry and enzyme-linked immunosorbent assay (ELISA). The supernatants which can detect human CD26 by both flow cytometry and ELISA were finally screened for immunostaining of formalin-fixed paraffin-embedded human tissue sections. The hybridomas were cloned by limiting dilution and culture medium was exchanged for serum-free GIT medium (Wako Pure Chemicals, Osaka, Japan). Monoclonal antibodies were purified from the supernatants using Protein A IgG Purification Kit (Pierce, Rockford, IL) according to the manufacturer's instructions.

Flow cytometry

A CD26-negative Jurkat T cell line (Jurkat parent) and a stable Jurkat T cell line transfected with human CD26

cDNA (Jurkat-CD26WT) described previously [24] were used for screening of hybridomas. Cells were washed in PBS containing 1% FBS, 1 mM EDTA and 0.1% sodium azide, and incubated with 100 μl of hybridoma supernatant or 20 μg/ml of purified mouse anti-human CD26 mAb for 25 min at 4°C, and subsequently stained with PE-conjugated goat anti-mouse Ig pAb (BD Biosciences, San Jose, CA) for 25 min at 4°C. Acquisition was performed using FACSCalibur (BD Biosciences) and data were analyzed with FlowJo software (Tree Star, Ashland, OR). For cross-blocking studies of humanized anti-CD26 mAb (YS110), cells were pretreated with unlabeled YS110 or control human IgG (50 μg/ml, respectively) for 25 min at 4°C, and subsequently incubated with 100 μl of hybridoma supernatant or 20 μg/ml of purified mouse anti-human CD26 mAb for 25 min at 4°C, and finally stained with PE-conjugated goat anti-mouse Ig pAb for 25 min at 4°C. For cross-blocking studies of murine anti-CD26 mAbs, cells were pretreated with unlabeled 4G8, 1F7, 5F8, 16D4B, 9C11 or mouse IgG_1 isotype control (50 μg/ml, respectively) for 25 min at 4°C, and subsequently stained with Alexa Fluor 647-labeled clone 18 or clone 19 or PE-conjugated goat anti-mouse Ig pAb for 25 min at 4°C.

ELISA

The 96-well immunoplates (NUNC, Roskilde, Denmark) were coated with native sCD26 or denatured sCD26 described above in carbonate bicarbonate buffer (200 ng/well, respectively) or buffer alone as a negative control at 4°C overnight. Each well of the plate was blocked with 3% bovine serum albumin (BSA, Sigma, St.Louis, MO) in PBS for 1 hour at RT, and then incubated with 3-fold diluted hybridoma supernatants or 5 μg/ml of purified mouse anti-human CD26 mAb or goat anti-human CD26 pAb for 1 hour at RT, and subsequently incubated with horseradish peroxidase (HRP)-conjugated goat anti-mouse Ig pAb (BD Biosciences) or HRP-conjugated donkey anti-goat IgG Ab (Santa Cruz Biotechnology, Santa Cruz, CA) for 1 hour at RT. Tetramethylbenzidine (TMB) Peroxidase Substrate (KPL, Gaithersburg, MD) was finally added to each well and the reaction was stopped by 2N H_2SO_4. The absorbance at 450 nm/570 nm was measured in a Microplate Reader (Bio-Rad, Hercules, CA) and data were analyzed with Microplate Manager 6 software (Bio-Rad).

Tissue specimens and immunohistochemical staining

Formalin-fixed paraffin-embedded tissue specimens of malignant mesothelioma and normal liver, kidney and prostate were used for positive controls in the immunohistochemical examination. The use of human sample from autopsy cases with hepatocellular carcinoma, renal cell carcinoma, prostate adenocarcinoma, colon adenocarcinoma and lung adenocarcinoma was generously permitted by the bereaved families. This study was approved by the Okayama Rosai Hospital ethical review board and the Keio University School of Medicine ethical review board, and the purpose of the study was explained to all patients and their written informed consent was obtained. All studies on human subjects were carried out according to the principles set out in the Declaration of Helsinki. Formalin-fixed paraffin-embedded tissue specimens were cut into 4-6 μm sections and deparaffinized. Antigen retrieval was performed by 1) autoclaving in 10 mM citrate buffer (pH 6.0) for 20 min at 120°C, 2) 0.05% trypsin for 15 min at 37°C, 3) 0.02% proteinase K for 10 min at 37°C, or 4) boiling in 10 mM citrate buffer (pH 6.0) for 10 min at 100°C, and the sections were treated with 0.3% H_2O_2 in methanol for 10 min at RT to inactivate endogenous peroxidase, then treated with 2.5% horse serum (Vector Laboratories, Burlingame, CA) for 10 min at RT to block non-specific binding of the secondary horse antibody. The sections were treated with 100 μl of hybridoma supernatants or purified mouse anti-human CD26 mAb or goat anti-human CD26 pAb for 2 hours at RT, and subsequently treated with HRP-conjugated horse anti-mouse Ig pAb or HRP-conjugated horse anti-goat IgG pAb (Vector Laboratories) for 30 min at RT. The reaction was visualized with 3, 3'-diaminobenzidine (DAB) (Dojindo Laboratories, Kumamoto, Japan), and the tissue sections were counterstained for nucleus with hematoxylin. To confirm the binding specificity of Abs to human CD26, the anti-human CD26 Ab (100 μg/ml) was gently rotated with 500 μg/ml of sCD26 at 4°C overnight, and after centrifugation, the supernatant was used instead of the primary anti-human CD26 Ab. Expression pattern of CD26 was evaluated and verified independently by two pathologists. The optical microscope images were taken using Axio Scope.A1 microscope (Carl Zeiss, Oberkochen, Germany).

Results

Screening of hybridoma cells

To develop a novel anti-CD26 mAb capable of binding to the denatured CD26, we immunized mice with CD26 protein denatured in urea buffer. To determine the denaturing condition, we incubated CD26 protein in 8 M urea buffer at RT for 30 min, 3 hours or 12 hours, and analyzed the binding of anti-CD26 mAb (clone 5F8) or anti-CD26 pAb (R&D Systems) to the urea treated CD26 protein by ELISA as described in Materials and Methods. This analysis showed the decrease in the absorbance when CD26 protein was incubated for 30 min in urea buffer, with additional decrease in absorbance at 3 hours of incubation, while there was barely noticeable difference between 3 hours of incubation and 12 hours

of incubation (data not shown). These data suggest that most of the CD26 proteins were denatured when incubated in 8 M urea buffer for more than 3 hours, and we used this urea-treated CD26 protein as an immunogen.

After the fusion of splenocytes and P3U1 myeloma cells, the culture supernatant was collected and screened for selective reactivity with human CD26. For the first screening of hybridoma cells, we used an endogenous CD26-deficit Jurkat cell line (Jurkat parent) and a stable Jurkat cell line transfected with full-length human CD26 (Jurkat-CD26WT), and the binding to human CD26 was analyzed by flow cytometry. As shown in Figure 1A, we obtained a number of hybridomas secreting antibodies, some of which could stain Jurkat-CD26WT with bright intensity and others could stain with intermediate or dull intensity (red lines) while Jurkat parent cells showed no staining with all of these supernatants (blue lines). These data indicate that this screening method excludes

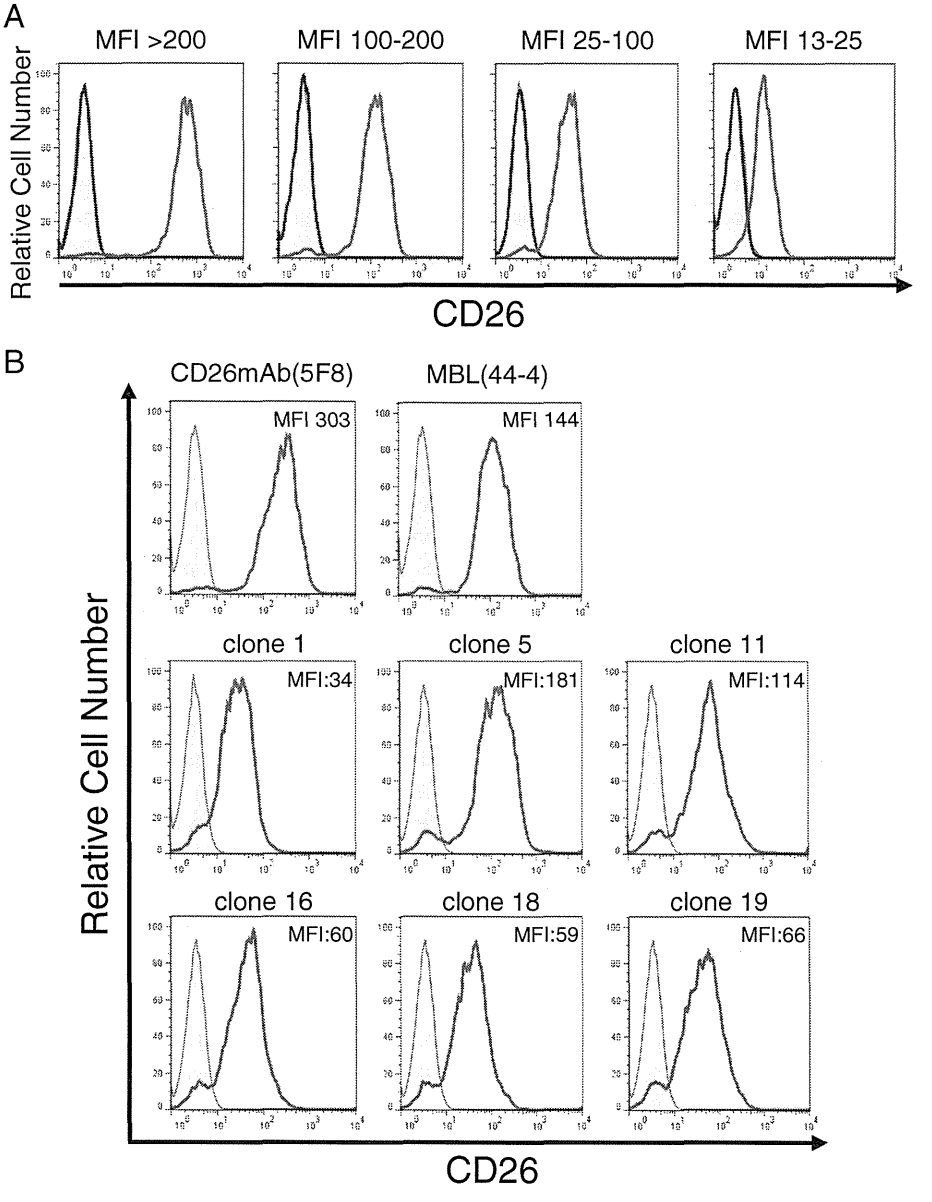

Figure 1 Flow cytometry analysis with novel anti-CD26 mAbs. A. Jurkat-CD26WT cells (red lines) or Jurkat parent cells (blue lines) were incubated with the hybridoma supernatant, and subsequently stained with PE-labeled anti-mouse Ig pAb, and analyzed by flow cytometry. **B.** Jurkat-CD26WT cells were incubated with the hybridoma supernatant (clone 1, 5, 11, 16, 18 or 19) or purified mouse anti-CD26 mAb (5F8) or commercial mouse anti-CD26 mAb (MBL, clone 44–4), and subsequently stained with PE-labeled anti-mouse Ig pAb, and analyzed by flow cytometry. The gray areas in each histogram show the data involving the isotype control. The mean fluorescence intensity (MFI) of each staining is shown. Data shown are repeated twice **(A)** and five times **(B)** with similar results.

the possibility of non-specific binding to other proteins beside CD26. The representative histograms of these novel anti-CD26 mAbs available for immunohistochemical staining were shown in Figure 1B.

The positive supernatants were then screened by ELISA for reactivity with native or denatured (urea treated) sCD26 protein. To exclude the possibility of non-specific binding to BSA used for blocking, we prepared the wells coated with buffer alone (without sCD26), subsequently blocked with BSA and incubated with hybridoma supernatants. The absorbance of the wells at 450 nm was subtracted from the absorbance of the wells coated with native or denatured sCD26. The clone was judged to be positive if the absorbance to the native sCD26 was higher than 0.1. The absorbance to the native or denatured sCD26 was quite different from clone to clone, and the representative absorbance of novel anti-CD26 mAbs available for immunohistochemical staining was shown in Figure 2. When sCD26 was denatured in urea buffer, the absorbance of 5F8, which cannot detect denatured CD26 in formalin-fixed tissues, was apparently decreased, while the absorbance of commercial mAb (purchased from MBL) or pAb (purchased from R&D Systems) was comparatively maintained (Figure 2). Although the decrease of absorbance to the denatured sCD26 was also observed with the novel anti-CD26 mAbs, particularly with clone 1, clone 11 and clone 16, the absolute value of absorbance to the denatured sCD26 was much higher than that of 5F8, except for clone 11 (Figure 2). As a result of the screening, 31 clones that secreted anti-human CD26 mAbs were evaluated for both flow cytometry and ELISA.

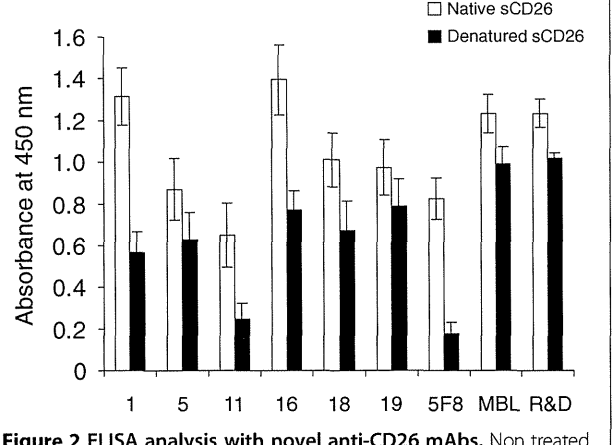

Figure 2 ELISA analysis with novel anti-CD26 mAbs. Non treated native soluble CD26 (sCD26) or urea treated denatured sCD26 was incubated with the hybridoma supernatant (clone 1, 5, 11, 16, 18 or 19) or purified mouse anti-CD26 mAb (5F8) or commercial mouse anti-CD26 mAb (MBL, clone 44–4) or purified goat anti-CD26 pAb (R&D Systems). The absorbance at 450 nm/570 nm was measured, and data are shown as mean ± S.E. from three independent experiments.

Immunohistochemical staining with novel anti-CD26 mAbs

To determine whether the newly developed anti-CD26 mAbs were suitable for immunohistochemical staining of CD26 in formalin-fixed tissue sections, surgically resected tissue specimens of normal liver, kidney, prostate, and malignant mesothelioma were immunostained with these mAbs, with commercial anti-CD26 mAb (purchased from MBL) and anti-CD26 pAb (purchased from R&D Systems) being used as controls. Although we examined several antigen retrieval conditions, tissue specimens stained with anti-CD26 mAb purchased from MBL exhibited only a slightly positive reaction with weak staining intensity, revealing this mAb to be inappropriate for the detection of CD26 expression in formalin-fixed clinical samples (Figure 3A-i). In contrast, tissue specimens stained with anti-CD26 pAb purchased from R&D Systems exhibited a clear staining pattern of CD26, namely the surface membrane of bile canaliculi, the brush border of renal proximal tubular epithelial cells and prostate epithelial cells were specifically stained with low background (Figure 3A-ii). We have previously shown that CD26 was also highly expressed in various pathologic types of malignant mesothelioma, including localized malignant mesothelioma, well-differentiated papillary malignant mesothelioma, and diffuse malignant mesothelioma [16], and the specific staining of malignant meshothelioma cells was also observed with the use of the anti-CD26 pAb (Figure 3A-ii). After testing the hybridoma supernatants from the 31 clones described above for immunohistochemical staining, we finally obtained 6 clones (clone 1, 5, 11, 16, 18 or 19) capable of staining CD26 in formalin-fixed tissues with much stronger intensity than the mAb purchased from MBL. As shown in Figure 3A, tissue specimens stained with two representative clones (clone 18 or 19) exhibited reliable staining pattern and intensity comparable to the pAb purchased from R&D Systems (panels iii and iv), while no apparent staining of CD26 was observed in the specimens stained with clone 3 (judged to be negative for immunostaining) (panel v). Representative results of immunostaining with the other 4 clones (clone 1, 5, 11 or 16) were shown in Additional file 1: Figure S1.

We next examined immunohistochemical staining with purified novel mAbs instead of the hybridoma culture supernatants. To determine the optimal Ab concentration for immunostaining, we evaluated the anti-human CD26 Abs in concentrations ranging from 1 μg/ml to 100 μg/ml. As shown in Figure 3B, staining of malignant mesothelioma cells was hardly observed with 1 μg/ml of clone 18, clone 19 mAb or pAb purchased from R&D Systems, while the staining intensity was enhanced in a dose-dependent manner up to 100 μg/ml of these three Abs (panels i, ii, iii).

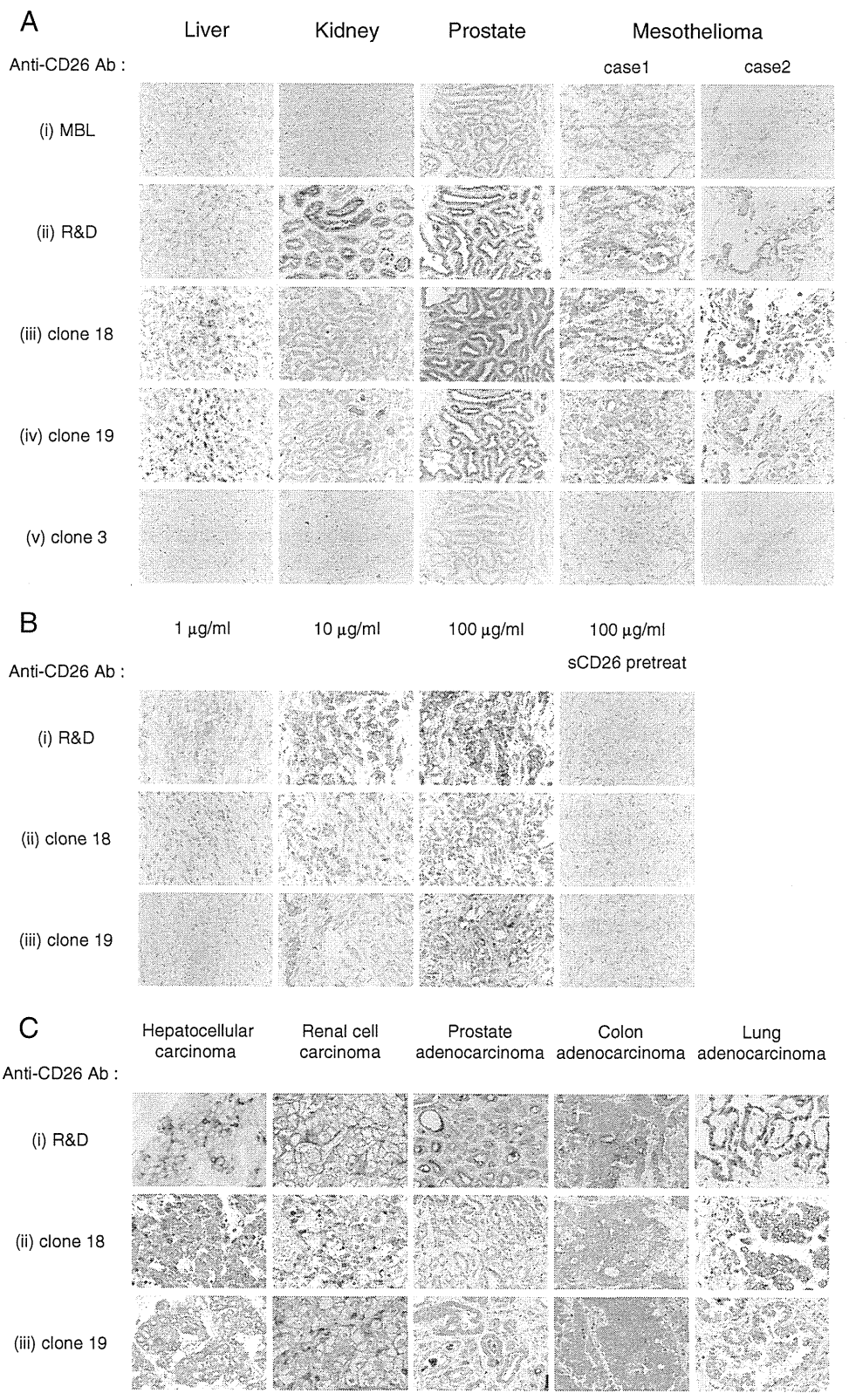

Figure 3 (See legend on next page.)

(See figure on previous page.)
Figure 3 Representative results of immunostaining with novel anti-CD26 mAbs. A. The tissue specimens of liver, kidney, prostate or two cases of malignant mesothelioma were stained with 100 μl of commercial mouse anti-human CD26 mAb supernatant (MBL, clone 44–4) (i), or 10 μg/ml of purified goat anti-human CD26 pAb (R&D Systems) (ii), or newly developed hybridoma supernatant (clone 18 (iii), clone 19 (iv) or clone 3 (v)). **B.** Malignant mesothelioma tissue specimens were stained with commercial goat anti-human CD26 pAb (R&D Systems) (i), or purified novel mouse anti-human CD26 mAbs (clone 18 (ii) or clone 19 (iii)) at the indicated concentrations of Abs in the presence or absence of sCD26. **C.** The tissue specimens of hepatocellular carcinoma, renal cell carcinoma, prostate adenocarcinoma, colon adenocarcinoma or lung adenocarcinoma were stained with 100 μg/ml of commercial goat anti-human CD26 pAb (R&D Systems) (i), or purified mouse anti-human CD26 mAbs (clone 18 (ii) or clone 19 (iii)). All specimens were counterstained with hematoxylin (original magnification, 200X).

Meanwhile, staining of tissues with even higher Ab concentrations resulted in similar intensity as compared with those stained with 100 μg/ml of the Abs (data not shown). In addition, to confirm the binding specificity of these Abs to human CD26, the sections were treated with purified anti-human CD26 Ab preincubated with sCD26. As shown in Figure 3B, the binding of these Abs was completely inhibited by sCD26 (panels i, ii, iii). These results indicate that the newly developed mAbs specifically bind to human CD26, and 100 μg/ml seems to be an optimal concentration of these Abs for immunohistochemical staining.

We further examined immunohistochemical staining of CD26-expressing tumor tissues other than malignant mesothelioma (hepatocellular carcinoma, renal cell carcinoma, prostate adenocarcinoma, colon adenocarcinoma, and lung adenocarcinoma) with the purified mAb of clone 18 or 19. As shown in Figure 3C, each tumor tissue stained with clone 18 or 19 (panels ii and iii) exhibited clarity and intensity similar to the levels observed with the anti-CD26 pAb purchased from R&D Systems (panel i). Results from the immunostaining studies indicate that CD26 can be detected both on the cell surface as well as cytoplasm of these carcinoma tissues.

Cross-blocking studies with humanized anti-CD26 mAb

In addition to detecting CD26 expression on tumor cells or lymphocytes prior to the therapeutic administration of humanized anti-CD26 mAb, it is also important to evaluate whether anti-CD26 mAb therapy affects CD26 expression on relevant tissues. For this purpose, we next examined the binding competitiveness of the 6 novel anti-CD26 mAbs with the humanized anti-CD26 mAb YS110. Jurkat-CD26WT was pretreated with unlabeled YS110 or control human IgG for 25 min, subsequently incubated with hybridoma supernatants, and stained with PE-labeled anti-mouse Ig pAb. As shown in Figure 4 (representative histograms are shown in Additional file 1: Figure S2), binding of YS110 or 1F7 to CD26 was completely blocked by YS110 while the binding of 5F8 to CD26 was hardly affected, indicating that YS110 was sufficiently bound to CD26. Although binding of clone 1, 11, 16 or 19 to CD26 was hardly affected by YS110 pretreatment, binding of clone 5 was partially inhibited, and binding of clone 18 was completely inhibited by YS110 (Figure 4 and Additional file 1: Figure S2). Taken together, these data suggest that clone 19 was capable of detecting denatured CD26 in formalin-fixed tissue sections with the most reliable staining pattern and intensity, exhibited no cross-reactivity with YS110, and was suitable for analysis of CD26 expression on clinical samples following the administration of YS110.

Epitope mapping of novel anti-CD26 mAbs

To define the CD26 epitope recognized by clone 18 and 19, we conducted cross-blocking studies using anti-CD26 mAbs with epitopes that had been extensively characterized previously as described in Materials and Methods [18]. To confirm the binding of anti-CD26 mAbs to CD26, Jurkat-CD26WT was incubated with unlabeled 4G8, 1F7, 5F8, 16D4B, 9C11 or mouse IgG_1 isotype control for 25 min, and subsequently stained with PE-labeled anti-mouse Ig pAb. As shown in Figure 5-i, each anti-CD26 mAb was sufficiently bound to CD26

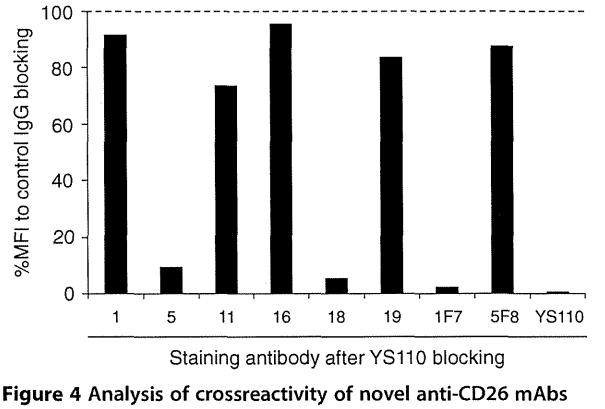

Figure 4 Analysis of crossreactivity of novel anti-CD26 mAbs with humanized anti-CD26 mAb. Jurkat-CD26WT cells were pretreated with unlabeled humanized anti-CD26 mAb (YS110) or human control IgG, and then treated with the hybridoma supernatant (clone 1, 5, 11, 16, 18 or 19) or purified mouse anti-CD26 mAb (1F7 or 5F8), and subsequently stained with PE-labeled anti-mouse Ig pAb. For staining with humanized anti-CD26 mAb, cells were stained with Alexa Fluor 647-labeled YS110 after pretreatment with unlabeled YS110. Data were analyzed by flow cytometry, and the percentage of mean fluorescence intensity (MFI) after YS110 blocking to MFI after control IgG blocking is shown. Data shown are repeated twice with similar results.

(blue lines), while there was no binding of the isotype control (red line). Modulation of cell surface CD26 into the cytoplasm following treatment with these anti-CD26 mAbs did not occur under these experimental conditions. Similarly, Jurkat-CD26WT was pretreated with unlabeled anti-CD26 mAbs, and subsequently stained with Alexa Fluor 647-labeled clone 18 or 19. As shown in Figure 5, binding of clone 18 or 19 to CD26 was completely inhibited by 1F7 (panels ii) or 4G8 (panels iii), respectively, with no effect by the other anti-CD26 mAbs. These results suggest that the epitope defined by clone 18 might be identical to 1F7, locating between the 248-358th AAs region of CD26, while the epitope defined by clone 19 might be identical to 4G8, locating between the 1-247th AAs region of CD26.

For cross-blocking studies involving the other 4 novel anti-CD26 mAbs, Jurkat-CD26WT was incubated with unlabeled clone 1, 5, 11, 16, 18, 19 or mouse IgG_1 isotype control for 25 min, and subsequently stained with Alexa Fluor 647-labeled 4G8, YS110, 5F8, 16D4B or 9C11. As shown in Additional file 1: Figure S3, binding of 4G8 to CD26 was completely blocked by clone 19, and binding of YS110 to CD26 was completely inhibited by clone 18 and partially inhibited by clone 5, consistent with the results shown in Figures 4 and 5. Clone 1 blocked completely the binding of 9C11 and partially the binding of 16D4B to CD26, while clone 16 completely inhibited the binding of both 9C11 and 16D4B to CD26 (Additional file 1: Figure S3). On the other hand, clone 11 inhibited the binding of 5F8 to CD26 completely (Additional file 1: Figure S3). These results strongly suggest that the novel anti-CD26 mAbs have a wide range of epitopes and can be broadly divided into 4 separate groups; the epitope of clone 19 being similar to 4G8, the epitopes of clone 5 and 18 being similar to 1F7 and YS110, the epitope of clone 11 being similar to 5F8, and the epitopes of clone 1 and 16 being similar to 9C11 (clone 16 is also similar to 16D4B).

To further confirm the epitope involved in binding of clone 18 and 19 to human CD26, we tested the ability of these two mAbs to bind to CD26 deletion mutants by flow cytometry [18]. We first tested the binding of the previously

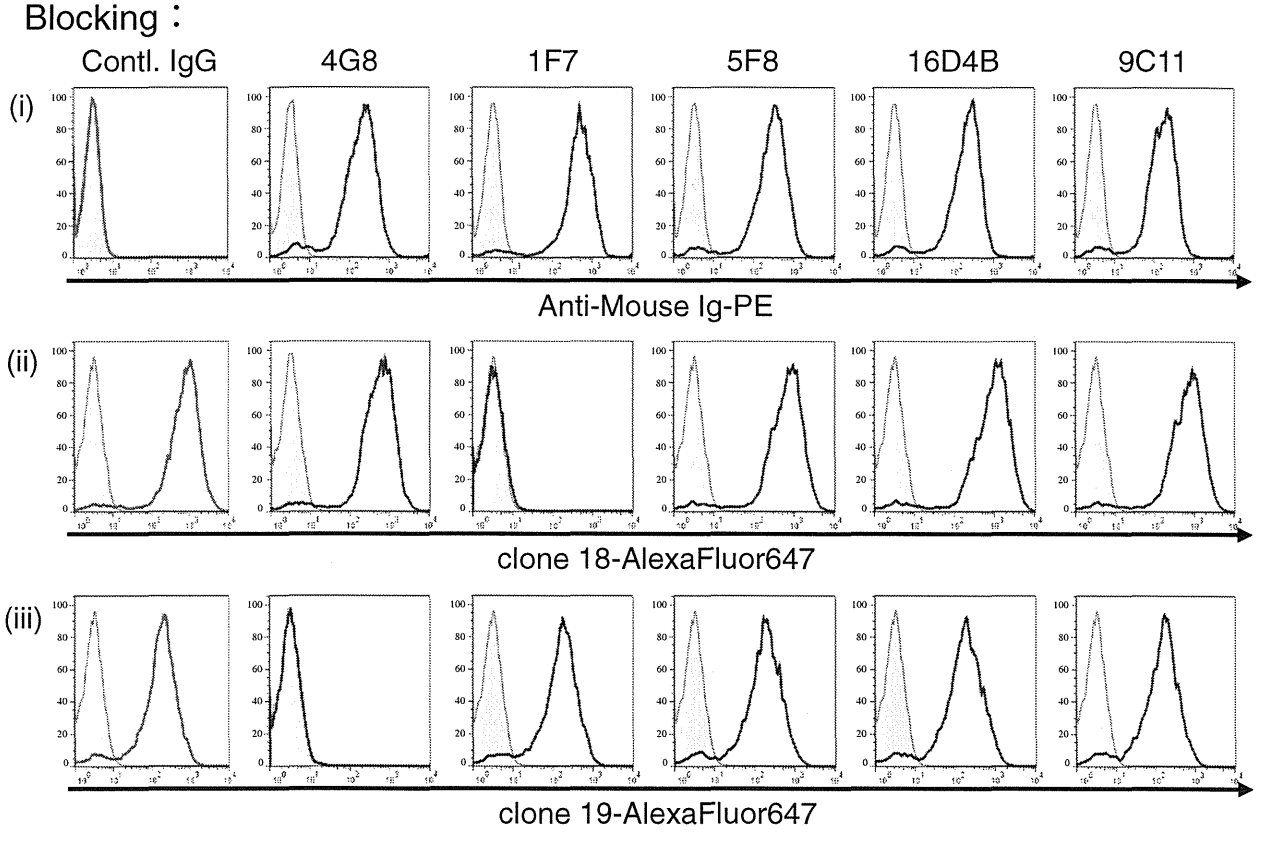

Figure 5 Blocking experiment of novel anti-CD26 mAb binding to CD26. Jurkat-CD26WT cells were pretreated with unlabeled mouse anti-CD26 mAbs (4G8, 1F7, 5F8, 16D4B, or 9C11) (blue lines) or mouse IgG_1 isotype control (Contl. IgG) (red lines), and subsequently stained with PE-labeled anti-mouse Ig pAb **(i)** or Alexa Fluor 647-labeled anti-CD26 mAbs (clone 18 **(ii)** or clone 19 **(iii)**), and analyzed by flow cytometry. The representative histograms of CD26 expression are shown, and the gray areas in each histogram show the data involving the isotype control. Data shown are repeated twice with similar results.

developed anti-human CD26 mAbs, 4G8, 1F7, or 5F8 to confirm the expression pattern of CD26 deletion mutants on COS-7 cells. As shown in Additional file 1: Figure S4, 4G8 recognized full-length CD26 and all 5 CD26 deletion mutants while 1F7 or 5F8 lost the ability to recognize the CD26 molecule with deletion from the 248th AA or from the 359th AA, respectively, indicating that the expression patterns of CD26 deletion mutants were identical to those reported previously [18]. We then analyzed the binding of YS110, clone 18 and clone 19 to the CD26 deletion mutants. As shown in Figure 6 (representative histograms are shown in Additional file 1: Figure S4), both YS110 and clone 18 recognized full length CD26, the 1-739th AAs region of CD26, the 1-577th AAs region of CD26, the 1-449th AAs region of CD26 and the 1-358th AAs region of CD26, but lost the ability to recognize the CD26 molecule with deletion from the 248th AA, suggesting that the sequence of the 248-358th AAs region on CD26 might be important for binding of YS110 and clone 18. On the other hand, clone 19 recognized full-length CD26 and all 5 CD26 deletion mutants, suggesting that the epitope defined by clone 19 might be located between the 1-247th AA region (Figure 6 and Additional file 1: Figure S4). YS110, clone 18 and clone 19 did not bind to COS-7 cells transfected with vector alone (mock) (Figure 6 and Additional file 1: Figure S4). Taken together, results from the cross-blocking studies and those involving CD26 deletion mutants strongly suggest that the epitope defined by clone 19 may be located between the 1-247th AAs region, and the epitope defined by clone 18 between the 248-358th AAs region, being almost identical to YS110.

Discussion

Although anti-human CD26 mAbs which we have developed previously or commercially available mAbs cannot clearly detect denatured CD26 in formalin-fixed paraffin-embedded tissues, the anti-human CD26 pAb purchased from R&D Systems is able to stain CD26 with reliable clarity and intensity. However, it is of concern that the staining pattern and intensity may differ among different lots of the anti-CD26 pAb. Since treatment with targeted therapeutic agents depends on the ability to reliably detect the appropriate targets on clinical samples, uniformity of the diagnostic reagents is critical, suggesting that pAbs that are used as research reagents are not appropriate for diagnostic uses in the clinical setting. In the present study, we describe the successful development of novel anti-human CD26 mAbs by immunizing mice with CD26 protein denatured in urea buffer that can potentially be used as diagnostic reagents clinically.

In an attempt to improve diagnostic accuracy, markers used for immunohistochemistry have been studied, such as galectin-3, HBME-1 and CK-19 for diagnosis of benign and malignant thyroid lesions [25,26], and FAP-α and Calponin for diagnosing whether ductal carcinoma in situ has microinvasion [27]. CD26 is highly expressed on the surface of malignant mesothelioma cells especially tumors of the epitheloid and biphasic types, but not on benign mesothelial tissues [16,17]. It has been recently reported that the expression level of CD26 in prostate cancer tissues is higher than that of normal prostatic tissues and increased with prostate cancer stage advancement, and CD26 expression is correlated with prostate specific antigen, suggesting that CD26 may be a good marker for prostate cancer diagnosis [28]. Furthermore, the overall survival of patients with CD26-positive GISTs is worse than that of patients with CD26-negative GISTs, suggesting that CD26 appears to be a reliable biomarker of malignant GIST of the stomach [29]. These observations strongly suggest that immunohistochemical

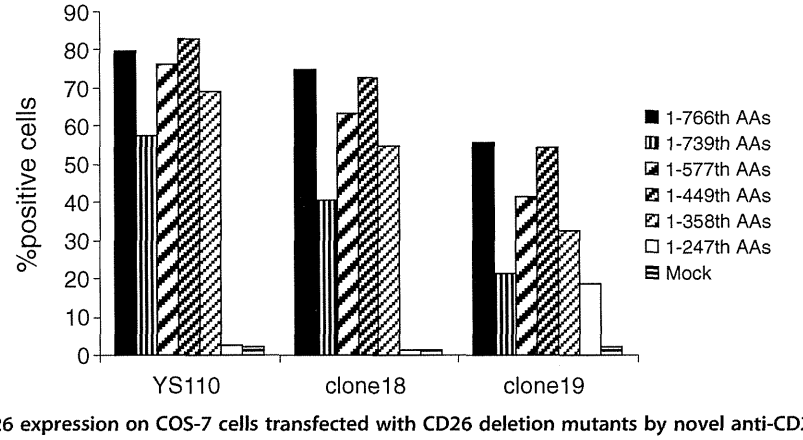

Figure 6 Staining for CD26 expression on COS-7 cells transfected with CD26 deletion mutants by novel anti-CD26 mAbs. cDNA of deleted CD26 was cotransfected with GFP-expressing plasmid to COS-7 cells. After 24 h, the transfected cells were stained with Alexa Fluor 647-labeled anti-CD26 mAbs (YS110, clone 18 or clone 19) or isotype control, and analyzed by flow cytometry. Following gating for GFP positive cells among all acquired cells, the percentage of CD26 positive cells was analyzed. Data shown are repeated twice with similar results.

staining of CD26 in formalin-fixed tumor tissues is important for diagnosis and prognosis of various tumors.

Since several anti-human CD26 mAbs such as Ta1, 1F7, 5F8 and 14D10 that were already developed in our laboratory by immunizing mice with a CD26 positive human T cell line (EL156) or a PHA-stimulated *Aotus trivirgatus* T cell line or a murine pre-B human CD26 transfectant (300–19) cannot clearly detect CD26 in formalin-fixed tissues [1,8,18], it was our hypothesis that utilizing human CD26 protein but not human CD26 positive cells as an immunogen would be important for the development of mAbs capable of recognizing the denatured CD26 molecule. Similar to CD26, only pAbs could react to the denatured HLA class I molecules in formalin-fixed paraffin-embedded tissues. Torigoe et al. recently succeeded in developing a novel anti-pan HLA class I mAb suitable for immunohistochemical staining of fixed tissues by immunizing a recombinant HLA-A protein denatured in urea buffer [30]. The exact role played by urea treatment of the CD26 protein in expanding the repertoire of the obtained anti-CD26 mAs is not yet clear, since we have not examined for potential differences in the characteristics of mAbs obtained after immunizing mice with urea-treated sCD26 protein or non-treated native sCD26 protein in this study. However, as shown in Figures 2 and 3, tissue specimens stained with anti-CD26 mAb purchased from MBL exhibited only a partially positive reaction with weak staining intensity, while this mAb showed higher absorbance to the urea treated sCD26 protein than the absorbance obtained from the novel anti-CD26 mAbs capable of staining CD26 with strong intensity in fixed tissues. These data strongly suggest that the structure of CD26 denatured by the method of antigen retrieval after formalin-fixation is quite different from that of CD26 denatured by urea buffer, and also suggest that anti-CD26 mAbs suitable for immunohistochemistry may be obtained more efficiently by immunizing mice with CD26 protein denatured by methods other than urea treatment, such as treatment with guanidine hydrochloride or sodium dodecyl sulfate (SDS), or with proteases such as trypsin or proteinase K, or by boiling. Further studies are needed to clarify the issue involving pretreatment of the immunogens and the characteristics of mAbs obtained after immunization.

In the present study, we have succeeded in developing novel anti-CD26 mAbs with a wide range of epitopes (Figures 5, 6 and Additional file 1: Figure S3). Since most of these novel mAbs completely inhibited the binding of the anti-CD26 mAbs (4G8, 1F7, 5F8, 16D4B or 9C11) developed previously by our group, the epitopes defined by these novel mAbs are expected to be similar to those recognized by the earlier mAbs. However, these novel anti-CD26 mAbs are capable of detecting denatured CD26 in fixed tissues with strong intensity, unlike the previously developed mAbs. Similarly, while clone 18 and YS110 recognize the similar epitope on CD26 (Figure 4, Additional file 1: Figure S2 and Additional file 1: Figure S3), only clone 18 can stain CD26 clearly in fixed tissues with strong intensity, suggesting that slight differences in the recognized epitopes can determine whether mAb binding to its denatured antigen can occur.

Cross-blocking studies showed that, in contrast to clone 5 or 18, the binding of clone 1, 11, 16 or 19 to CD26 was hardly affected by the humanized anti-CD26 mAb YS110 (Figure 4, Additional file 1: Figure S2 and Additional file 1: Figure S3), suggesting that these 4 novel anti-CD26 mAbs are suitable for analyzing CD26 expression in clinical samples following YS110 therapy. Potential uses of these novel mAbs in the clinical setting may be to detect CD26 expression in formalin-fixed tissues, or on circulating cells in blood samples, or sCD26 levels in bodily fluids through such methods as immunohistochemistry, flow cytometry, or ELISA. Furthermore, these novel mAbs are potentially useful for analyzing CD26 expression in fixed tissues or on the surface of lymphocytes or tumors during or following the administration of humanized anti-CD26 mAb in animal disease models that involve inoculated human lymphocytes or tumors [12,16], and are expected to contribute to future CD26-related research effort.

Since we intend to utilize these novel anti-CD26 mAbs as companion diagnostic agents in the clinical setting, our current effort is focused on improving immunohistochemical staining methods by examining such issues as the condition of antigen retrieval or blocking, or the optimal concentration of the primary antibody (anti-CD26 mAb) that can maximize staining intensity while lowering background staining. Furthermore, we also identified the amino acid sequence of the variable region in both the heavy chain and light chain of clone 19 (data not shown), and will aim to refine the ability of this mAb to bind to CD26 through genetic engineering techniques.

In conclusion, we have succeeded in developing novel anti-human CD26 mAbs suitable for immunohistochemical staining of CD26 in formalin-fixed tissue sections with reliable clarity and intensity. Furthermore, since some of these mAbs exhibit no cross-reactivity with the therapeutic humanized anti-CD26 mAb, they are potentially useful as companion diagnostic agents in the clinical setting while advancing future CD26-related research.

Additional file

Additional file 1: Figure S1. Representative results of immunostaining with novel anti-CD26 mAbs. The tissue specimens of liver, kidney, prostate or two cases of malignant mesothelioma were stained with

the hybridoma supernatant (clone 1, 5, 11 or 16), counterstained with hematoxylin (original magnification, 200X). **Figure S2.** Analysis of crossreactivity of novel anti-CD26 mAbs with humanized anti-CD26 mAb. Jurkat-CD26WT cells were pretreated with unlabeled humanized anti-CD26 mAb (YS110) (blue lines) or human control IgG (red lines), and then treated with the hybridoma supernatant (clone 1, 5, 11, 16, 18 or 19) or purified mouse anti-CD26 mAb (1F7 or 5F8), and subsequently stained with PE-labeled anti-mouse Ig pAb, or stained with Alexa Fluor 647-labeled YS110. Data were analyzed by flow cytometry, and the representative histograms are shown. The gray areas in each histogram show the data of isotype control. **Figure S3.** Blocking experiment of novel anti-CD26 mAb binding to CD26. Jurkat-CD26WT cells were pretreated with the hybridoma supernatant (clone 1, 5, 11, 16, 18 or 19) (blue lines) or mouse IgG_1 isotype control (Contl. IgG) (red lines), and subsequently stained with Alexa Fluor 647-labeled anti-CD26 mAbs or PE-labeled anti-mouse Ig pAb, and analyzed by flow cytometry. The representative histograms are shown, and the gray areas in each histogram show the data of isotype control. Data shown are repeated twice with similar results. **Figure S4.** Staining for CD26 expression on COS-7 cells transfected with CD26 deletion mutants by novel anti-CD26 mAbs. cDNA of deleted CD26 was cotransfected with GFP-expressing plasmid to COS-7 cells. After 24 h, the transfected cells were stained with Alexa Fluor 647-labeled anti-CD26 mAbs or isotype control, and analyzed by flow cytometry. The representative histograms of Alexa Fluor 647 were obtained by gating for GFP positive cells among all acquired cells, and the gray areas in each histogram show the data of isotype control.

Competing interests
The authors declare no competing financial interests associated with this manuscript.

Authors' contributions
RH and CM designed and coordinated the study. RH, TY, SM and EK conducted the experiments. CM, TY and KO supervised part of the experiments. All authors contributed to the interpretations and conclusions presented. RH and CM wrote the manuscript, and NHD, SI and HY participated in editing it. All authors read and approved the final manuscript.

Acknowledgements
The authors thank Ms. Hiroko Madokoro for excellent assistance with immunohistochemical staining of CD26, and also thank Ms. Haruna Otsuka and Ms. Aya Miwa for the assistance with preparation of soluble CD26 and the experiment of epitope mapping. This work was supported by Grant-in-Aid of The Ministry of Education, Science, Sports (KO and CM) and Culture, Ministry of Health, Labour, and Welfare, Japan (CM).

Author details
[1]Department of Therapy Development and Innovation for Immune Disorders and Cancers, Graduate School of Medicine, Juntendo University, 2-1-1, Hongo, Bunkyo-ku, Tokyo 113-8421, Japan. [2]Department of Pathology, Keio University School of Medicine, 35 Shinanomachi, Shinjuku-ku, Tokyo 160-8582, Japan. [3]Department of Pathology & Oncology, Juntendo University School of Medicine, 2-1-1, Hongo, Bunkyo-ku, Tokyo 113-8421, Japan. [4]Division of Hematology/Oncology, University of Florida, 1600 SW Archer Road- Box 100278, Room MSB M410A, Gainesville, FL 32610, USA.

Received: 3 October 2013 Accepted: 24 January 2014
Published: 6 February 2014

References
1. Fox DA, Hussey RE, Fitzgerald KA, Acuto O, Poole C, Palley L, Daley JF, Schlossman SF, Reinherz EL: **Ta1, a novel 105 KD human T cell activation antigen defined by a monoclonal antibody.** *J Immunol* 1984, **133**:1250–6.
2. Nanus DM, Engelstein D, Gastl GA, Gluck L, Vidal MJ, Morrison M, Finstad CL, Bander NH, Albino AP: **Molecular cloning of the human kidney differentiation antigen gp160: human aminopeptidase A.** *Proc Natl Acad Sci USA* 1993, **90**:7069–73.
3. Tanaka T, Camerini D, Seed B, Torimoto Y, Dang NH, Kameoka J, Dahlberg HN, Schlossman SF, Morimoto C: **Cloning and functional expression of the T cell activation antigen CD26.** *J Immunol* 1992, **149**:481–6.
4. Morimoto C, Schlossman SF: **The structure and function of CD26 in the T-cell immune response.** *Immunol Rev* 1998, **161**:55–70.
5. Ohnuma K, Dang NH, Morimoto C: **Revisiting an old acquaintance: CD26 and its molecular mechanisms in T cell function.** *Trends Immunol* 2008, **29**:295–301.
6. De Meester I, Korom S, Van Damme J, Scharpe S: **CD26, let it cut or cut it down.** *Immunol Today* 1999, **20**:367–75.
7. von Bonin A, Huhn J, Fleischer B: **Dipeptidyl-peptidase IV/CD26 on T cells: analysis of an alternative T-cell activation pathway.** *Immunol Rev* 1998, **161**:43–53.
8. Morimoto C, Torimoto Y, Levinson G, Rudd CE, Schrieber M, Dang NH, Letvin NL, Schlossman SF: **1 F7, a novel cell surface molecule, involved in helper function of CD4 cells.** *J Immunol* 1989, **143**:3430–9.
9. Masuyama J, Yoshio T, Suzuki K, Kitagawa S, Iwamoto M, Kamimura T, Hirata D, Takeda A, Kano S, Minota S: **Characterization of the 4C8 antigen involved in transendothelial migration of CD26(hi) T cells after tight adhesion to human umbilical vein endothelial cell monolayers.** *J Exp Med* 1999, **189**:979–90.
10. Ohnuma K, Inoue H, Uchiyama M, Yamochi T, Hosono O, Dang NH, Morimoto C: **T-cell activation via CD26 and caveolin-1 in rheumatoid synovium.** *Mod Rheumatol* 2006, **16**:3–13.
11. Hatano R, Ohnuma K, Yamamoto J, Dang NH, Morimoto C: **CD26-mediated co-stimulation in human CD8(+) T cells provokes effector function via pro-inflammatory cytokine production.** *Immunology* 2013, **138**:165–72.
12. Hatano R, Ohnuma K, Yamamoto J, Dang NH, Yamada T, Morimoto C: **Prevention of acute graft-versus-host disease by humanized anti-CD26 monoclonal antibody.** *Br J Haematol* 2013, **162**:263–77.
13. Havre PA, Abe M, Urasaki Y, Ohnuma K, Morimoto C, Dang NH: **The role of CD26/dipeptidyl peptidase IV in cancer.** *Front Biosci* 2008, **13**:1634–45.
14. Ho L, Aytac U, Stephens LC, Ohnuma K, Mills GB, McKee KS, Neumann C, LaPushin R, Cabanillas F, Abbruzzese JL, *et al*: **In vitro and in vivo antitumor effect of the anti-CD26 monoclonal antibody 1 F7 on human CD30+ anaplastic large cell T-cell lymphoma Karpas 299.** *Clin Cancer Res* 2001, **7**:2031–40.
15. Inamoto T, Yamochi T, Ohnuma K, Iwata S, Kina S, Inamoto S, Tachibana M, Katsuoka Y, Dang NH, Morimoto C: **Anti-CD26 monoclonal antibody-mediated G1-S arrest of human renal clear cell carcinoma Caki-2 is associated with retinoblastoma substrate dephosphorylation, cyclin-dependent kinase 2 reduction, p27(kip1) enhancement, and disruption of binding to the extracellular matrix.** *Clin Cancer Res* 2006, **12**:3470–7.
16. Inamoto T, Yamada T, Ohnuma K, Kina S, Takahashi N, Yamochi T, Inamoto S, Katsuoka Y, Hosono O, Tanaka H, *et al*: **Humanized anti-CD26 monoclonal antibody as a treatment for malignant mesothelioma tumors.** *Clin Cancer Res* 2007, **13**:4191–200.
17. Aoe K, Amatya VJ, Fujimoto N, Ohnuma K, Hosono O, Hiraki A, Fujii M, Yamada T, Dang NH, Takeshima Y, Inai K, Kishimoto T, Morimoto C: **CD26 overexpression is associated with prolonged survival and enhanced chemosensitivity in malignant pleural mesothelioma.** *Clin Cancer Res* 2012, **18**:1447–56.
18. Dong RP, Tachibana K, Hegen M, Scharpe S, Cho D, Schlossman SF, Morimoto C: **Correlation of the epitopes defined by anti-CD26 mAbs and CD26 function.** *Mol Immunol* 1998, **35**:13–21.
19. Yamada K, Hayashi M, Madokoro H, Nishida H, Du W, Ohnuma K, Sakamoto M, Morimoto C, Yamada T: **Nuclear localization of CD26 induced by a humanized monoclonal antibody inhibits tumor cell growth by modulating of POLR2A transcription.** *PLoS One* 2013, **8**:e62304.
20. Takebe Y, Seiki M, Fujisawa J, Hoy P, Yokota K, Arai K, Yoshida M, Arai N: **SR alpha promoter: an efficient and versatile mammalian cDNA expression system composed of the simian virus 40 early promoter and the R-U5 segment of human T-cell leukemia virus type 1 long terminal repeat.** *Mol Cell Biol* 1988, **8**:466–72.
21. Tanaka J, Miwa Y, Miyoshi K, Ueno A, Inoue H: **Construction of Epstein-Barr virus-based expression vector containing mini-oriP.** *Biochem Biophys Res Commun* 1999, **264**:938–43.
22. Tanaka T, Duke-Cohan JS, Kameoka J, Yaron A, Lee I, Schlossman SF, Morimoto C: **Enhancement of antigen-induced T-cell proliferation by soluble CD26/dipeptidyl peptidase IV.** *Proc Natl Acad Sci USA* 1994, **91**:3082–6.
23. Ikushima H, Munakata Y, Ishii T, Iwata S, Terashima M, Tanaka H, Schlossman SF, Morimoto C: **Internalization of CD26 by mannose 6-phosphate/insulin-like growth factor II receptor contributes to T cell activation.** *Proc Natl Acad Sci USA* 2000, **97**:8439–44.

24. Tanaka T, Kameoka J, Yaron A, Schlossman SF, Morimoto C: **The costimulatory activity of the CD26 antigen requires dipeptidyl peptidase IV enzymatic activity.** *Proc Natl Acad Sci USA* 1993, **90**:4586–90.
25. Saleh HA, Jin B, Barnwell J, Alzohaili O: **Utility of immunohistochemical markers in differentiating benign from malignant follicular-derived thyroid nodules.** *Diagn Pathol* 2010, **5**:9.
26. de Matos LL, Del Giglio AB, Matsubayashi CO, de Lima Farah M, Del Giglio A, da Silva Pinhal MA: **Expression of CK-19, galectin-3 and HBME-1 in the differentiation of thyroid lesions: systematic review and diagnostic meta-analysis.** *Diagn Pathol* 2012, **7**:97.
27. Hua X, Yu L, Huang X, Liao Z, Xian Q: **Expression and role of fibroblast activation protein-alpha in microinvasive breast carcinoma.** *Diagn Pathol* 2011, **6**:111.
28. Lu Z, Qi L, Bo XJ, Liu GD, Wang JM, Li G: **Expression of CD26 and CXCR4 in prostate carcinoma and its relationship with clinical parameters.** *J Res Med Sci* 2013, **18**:647–52.
29. Yamaguchi U, Nakayama R, Honda K, Ichikawa H, Hasegawa T, Shitashige M, Ono M, Shoji A, Sakuma T, Kuwabara H: **Distinct gene expression-defined classes of gastrointestinal stromal tumor.** *J Clin Oncol* 2008, **26**:4100–8.
30. Torigoe T, Asanuma H, Nakazawa E, Tamura Y, Hirohashi Y, Yamamoto E, Kanaseki T, Hasegawa T, Sato N: **Establishment of a monoclonal anti-pan HLA class I antibody suitable for immunostaining of formalin-fixed tissue: unusually high frequency of down-regulation in breast cancer tissues.** *Pathol Int* 2012, **62**:303–8.

doi:10.1186/1746-1596-9-30
Cite this article as: Hatano *et al.*: Establishment of monoclonal anti-human CD26 antibodies suitable for immunostaining of formalin-fixed tissue. *Diagnostic Pathology* 2014 **9**:30.

PLOS ONE

CD9 Negatively Regulates CD26 Expression and Inhibits CD26-Mediated Enhancement of Invasive Potential of Malignant Mesothelioma Cells

Toshihiro Okamoto[1,2], Satoshi Iwata[1,2], Hiroto Yamazaki[1,2], Ryo Hatano[1,2], Eriko Komiya[1], Nam H. Dang[3], Kei Ohnuma[1,2], Chikao Morimoto[1,2]*

1 Department of Therapy Development and Innovation for Immune disorders and Cancers, Graduate School of Medicine, Juntendo University, Tokyo, Japan, **2** Division of Clinical Immunology, Institute of Medical Science, University of Tokyo, Tokyo, Japan, **3** Division of Hematology and Oncology, University of Florida Shands Cancer Center, Gainesville, Florida, United States of America

Abstract

CD26/dipeptidyl peptidase IV is a cell surface glycoprotein which consists of multiple functional domains beside its ectopeptidase site. A growing body of evidence indicates that elevated expression of CD26 correlates with disease aggressiveness and invasive potential of selected malignancies. To further explore the molecular mechanisms involved in this clinical behavior, our current work focused on the interaction between CD26 and CD9, which were recently identified as novel markers for cancer stem cells in malignant mesothelioma. We found that CD26 and CD9 co-modulated and co-precipitated with each other in the malignant mesothelioma cell lines ACC-MESO1 and MSTO-211H. SiRNA study revealed that depletion of CD26 led to increased CD9 expression, while depletion of CD9 resulted in increased CD26 expression. Consistent with these findings was the fact that gene transfer of CD26 into CD26-negative MSTO-211H cells reduced CD9 expression. Cell invasion assay showed that overexpression of CD26 or gene depletion of CD9 led to enhanced invasiveness, while CD26 gene depletion resulted in reduced invasive potential. Furthermore, our work suggested that this enhanced invasiveness may be partly mediated by α5β1 integrin, since co-precipitation studies demonstrated an association between CD26 and α5β1 integrin. Finally, gene depletion of CD9 resulted in elevated protein levels and tyrosine phosphorylation of FAK and Cas-L, which are downstream of β1 integrin, while depletion of CD26 led to a reduction in the levels of these molecules. Collectively, our findings suggest that CD26 potentiates tumor cell invasion through its interaction with α5β1 integrin, and CD9 negatively regulates tumor cell invasion by reducing the level of CD26-α5β1 integrin complex through an inverse correlation between CD9 and CD26 expression. Our results also suggest that CD26 and CD9 serve as potential biomarkers as well as promising molecular targets for novel therapeutic approaches in malignant mesothelioma and other malignancies.

Citation: Okamoto T, Iwata S, Yamazaki H, Hatano R, Komiya E, et al. (2014) CD9 Negatively Regulates CD26 Expression and Inhibits CD26-Mediated Enhancement of Invasive Potential of Malignant Mesothelioma Cells. PLoS ONE 9(1): e86671. doi:10.1371/journal.pone.0086671

Editor: Arun Rishi, Wayne State University, United States of America

Received September 18, 2013; **Accepted** December 12, 2013; **Published** January 23, 2014

Funding: This work was supported by grants-in aid from the Ministry of Education, Science, Sports and Culture (S.I. 24591442, K.O. 21679005, C.M. 24659401), and Ministry of Health, Labor and Welfare, Japan, and by the Program for Promotion of Fundamental Studies in Health Sciences of the National Institute of Biomedical Innovation (C.M. 07-17). The funders had no role in study design, data collection and analysis, decision to publish, or preparation of the manuscript.

Competing Interests: C. Morimoto is a patent holder of humanized CD26 monoclonal antibody (name of patent: Anti-CD26 antibodies and Methods of use thereof. Number of patent: US Patent # 7402698). Y's therapeutics,Inc owns this patent and C. Morimoto is one of founders of this company. C. Morimoto declares that this does not alter the authors' adherence to all PLOS ONE policies on sharing data and materials as detailed online in the guide for authors.

* E-mail: morimoto@ims.u-tokyo.ac.jp

Introduction

Malignant pleural mesothelioma is an aggressive malignancy arising from the mesothelial cells lining the pleura [1]. It is generally associated with a history of asbestos exposure and has a very poor prognosis [1]. In fact, the median survival is less than 12 months, with most patients dying within 10 to 17 months of their first symptoms. Moreover, the incident of malignant mesothelioma has increased in industrialized nations as a result of past widespread exposure to asbestos [2].

CD26 is a 110-kDa cell surface glycoprotein with known dipeptidyl peptidase IV (DPPIV; EC 3.4.14.5) activity in its extracellular domain [3] and is capable of cleaving N-terminal dipeptides with either L-proline or L-alanine at the penultimate position [3]. CD26 activity is dependent on cell type and the microenvironment factors that can influence its multiple biological roles [3–6]. Association with various proteins, including fibroblast-activation protein-α, plasminogen, adenosine deaminase, CD45 and collagen, influences its activity [3]. As a result of its various interactions, CD26 has an important, but complex, function in cellular behavior, with its biologic effect dependent on the cell type and the microenvironment.

Likely, as a result of this multifunctional characteristic, CD26 is associated with a high level of clinical aggressiveness in some tumors but a lower level in others [7,8]. For example, it is a marker of aggressive disease for certain subsets of T-cell non-Hodgkin lymphomas/leukemias, with expression of CD26 on T-lymphoblastic lymphomas/acute lymphoblastic leukemia cells being associated with a worse outcome compared with CD26-negative tumors [9]. CD26 is also expressed at high levels on renal

carcinoma cells [10]. In an immunohistochemical analysis of 152 patients with gastrointestinal stromal tumors (GIST), CD26 was found to be associated with a poorer overall survival [11]. In addition, CD26 can serve as a prognostic marker in B-cell chronic lymphocytic leukemia [12]. Furthermore, CD26 itself may be a novel therapeutic target. Anti-CD26 monoclonal antibody (mAb) treatment resulted in both *in vitro and in vivo* antitumor activity against several tumor types, including lymphoma and renal cell carcinoma [13,14]. Our recent work showed that CD26 is preferentially expressed on malignant mesothelioma cells but not on normal mesothelial cells, and suggested that membranous expression of CD26 is of potential importance in the treatment of mesothelioma patients [15]. Importantly, humanized anti-CD26 antibody inhibited growth of malignant mesothelioma cells and induced long-term survival of tumor-transplanted immunodeficient mice [16].

CD9, a member of the tetraspanin superfamily, has been implicated in the regulation of various physiological processes, including cell motility, adhesion and fusion through an association with integrin family proteins [17]. CD9 was identified as a molecule that suppresses cellular motility and metastatic potential of a human lung adenocarcinoma cell line [18]. Clinicopathologic findings indicated that CD9 may be a predictor for better prognosis in lung adenocarcinoma [19].

While an inverse correlation between CD9 expression and metastatic development was observed in melanoma, cervical carcinoma and multiple myeloma, up-regulation of CD9 was demonstrated in aggressive gastric carcinoma [20] and high-grade astrocytic tumors [21]. The regulatory role of CD9 in cell motility therefore appears to be complex and may vary depending on the presence of an endothelial barrier and other factors.

More recently, we have identified CD9, CD24 and CD26 as cancer stem cell markers of malignant mesothelioma cells that correlated with primary stem cell signatures [22,23]. In addition, CD26 and CD9 have been reported to be associated with several cell surface molecules such as CD45, CXCR4, M6P/IGFIIR [3], and integrin family molecules [24], respectively.

Our present study focused on the molecular association between CD26 and CD9 and found that the interaction between these two molecules plays a significant role in invasiveness, motility, and proliferation of malignant mesothelioma cells.

Materials and Methods

Ethics Statement

All experiments using mice were approved by and carried out following the guidelines of the Institute Animal Care and Use Committee of the University of Tokyo (Tokyo, Japan). Details of approval and animal welfare considerations are described in Checklist S1.

Cell lines

Mesothelioma cell line ACC-MESO1 (MESO1) was obtained from RIKEN BioResource Center (Tsukuba, Japan). MSTO-211H (MSTO), NCI-H2452, and NCI-H226 were obtained from ATCC (Manassas, VA, USA). These cell lines were maintained in RPMI 1640 supplemented with 10% heat-inactivated fetal calf serum (FCS), penicillin (100 U/ml) and streptomycin (100 μg/ml) at 37°C and 5% CO_2.

Antibodies

Humanized anti-CD26 mAb and anti-CD9 mAb were developed in our laboratory [16,25]. Antibodies against integrin α1(rabbit polyclonal), α2(rabbit monoclonal EPR5788) and α3(rabbit polyclonal) were purchased from Abcam (Cambridge, UK), and mouse monoclonal antibodies against integrin α4 (3G6), α5 (2H6), α6 (2C3A), and β1 (4B4) were developed in our laboratory [26–28]. Mouse monoclonal antibody against FAK (10G2)and rabbit polyclonal antibody against Cas-L (TA248) were developed in our laboratory. Mouse monoclonal antibody against Cas-L was obtained from ImmuQuest (Seamer, UK). Anti-phosphotyrosine (pTyr) mouse monoclonal antibody (4G10) was produced from hybridoma obtained from ATCC. Anti-CD26 goat polyclonal antibody was purchased from R&D Systems (Minneapolis, MN, USA). For flow cytometric analysis, anti-CD26-FITC, anti-CD9-FITC, anti-CD9-PE were obtained from BD Biosciences (San Jose, CA, USA), and anti-CD26-FITC (5K78)(IgM) and FITC-conjugated antibody to mouse IgM were purchased from Santa Cruz Biotechnology, Inc. (Santa Cruz, CA, USA). The secondary antibodies against goat IgG (H+L), rabbit IgG (H+L), and mouse IgG (L) conjugated with HRP were obtained from Jackson ImmunoResearch Laboratories, Inc. (West Grove, PA, USA). Human IgG andanti-actin rabbit polyclonal antibody were purchased from Sigma-Aldrich Co. LLC (St. Louis, MO, USA) and Abcam, respectively.

Transfection of CD26 cDNA

MSTO-Wild cells were transfected with full-length cDNA of CD26 subcloned in retroviral plasmid pLNCX2 vector (Clontech, Mountain View, CA, USA) using the Lipofectamine reagent (Invitrogen, Carlsbad, CA, USA). Fresh RPMI 1640 with 10% FCS was replenished 19 h after transfection and cells were harvested after 48 h. As a control, cells were transfected with the pLNCX2 vector. Expression of the transfected cDNA was confirmed by immunoblotting and flow cytometry.

Small interfering RNAs and short hairpin RNAs for CD26 and CD9

To deplete endogenous CD26 mRNA, three small interfering (si) RNAs and two short hairpins (sh) RNAs were obtained from Qiagen (Hilden, Germany) or Sigma-Aldrich (reference sequence: NM_001935). The sequences are as follows.

CD26 siRNA-1: 5′-ACACTCTAACTGATTACTAA-3′,

CD26 siRNA-2: 5′-CAGTAAAGAGGCGAAGTATTA-3′

CD26 siRNA-3: 5′-ATCGGGAAGTGGCGTGTTCAA-3′

CD26 shRNA-1: 5′-CCGGGACTGAAGTTATACTCCTTAACTCGAGTTAAGGAGTATAACTTCAGTCTTTTTG-3′

CD26 shRNA-2: 5′-CCGGCCAATGCAACTTCCATACAAACTCGAGTTTGTATGGAAGTTGCATTGGTTTTTG-3′

To deplete endogenous CD9, two siRNAs and two shRNAs were used (reference sequence: NM_001769). The sequences are as follows.

CD9 siRNA-1: 5′-CGTGGAACAGTTTATCTCAT-3′

CD9 siRNA-2: 5′-AATTGCCGTGGTCATGATATT-3′

CD9 shRNA-1: 5′-CCGGGCTGTTCGGATTTAACTTCATCTCGAGATGAAGTTAAATCCGAACAGCTTTTTG-3′

CD9 shRNA-2: 5′-CCGGCACAAGGATGAGGTGATTAAGCTCGAGCTTAATCACCTCATCCTTGTGTTTTTG-3′

For controls, negative control siRNA (Qiagen) or non-target shRNA control (Sigma-Aldrich) was used.

Transfection of siRNAs and shRNAs

For assays involving siRNA, cells (3×10^4) were cultured for 24 h on 24-well plates and transfected with 22 nmol/L siRNA cocktail against CD26, CD9 or negative control siRNA using TransIT-TKO transfection reagents (Mirus Bio LLC, Madison, WI, USA). For shRNAs, lentiviral plasmid containing each shRNA above (MISSION shRNA; Sigma-Aldrich), or non-targeting control plasmid was co-transfected with ViraPower Lentiviral packaging mix to 293FT cells using Lipofectamine 2000 (Invitrogen). The mesothelioma cell lines were infected with the shRNA-expressing lentivirus, and stable cell lines were generated by selection with puromycin.

Flow cytometry and Fluorescence-activated cell sorting (FACS) analysis

Cells were stained with the monoclonal antibodies described above for 30 min on ice. For controls, cells were incubated with isotype-matched IgG. Cells were analyzed by BD FACSCalibur or sorted by BD FACSAria. Data were analyzed by FlowJo software (Tree Star, Inc., Ashland, OR, USA).

Microarray analysis

MESO1 cells transfected with control siRNA or CD26 siRNA were used to examine the effect of CD26 depletion. MSTO-Wild and MSTO-CD26 (+) cells were used to study the effect of CD26 overexpression. Total RNA was isolated using TRIzol (Invitrogen) and subjected to DNA microarray analysis with DNA Chip 3D Gene (TORAY, Yokohama, Japan). A heat map of tetraspanin genes differently expressed between CD26-depleted and CD26-overexpressed mesothelioma cells was constructed by hierarchical cluster analysis using cluster 3.0 software and the results were displayed with the TreeView program. The data discussed in this publication have been deposited in NCBI's Gene Expression Omnibus and are accessible through GEO Series accession number GSE52216.

Immunoblotting

Cells were collected and suspended in lysis buffer (50 mM HEPES, pH7.4, 150 mM NaCl, 1.0% Triton X-100, 30 mM sodium pyrophosphate, 50 mM NaF, 1 mM Na_3VO_4). The cell lysates were centrifuged at 15,000 rpm for 15 min at 4°C and the supernatants were stored at −80 °C or used for experiments directly. Ten micrograms of proteins were electrophoresed on SDS-PAGE and transferred to a polyvinylidene fluoride (PVDF) microporous membrane Immobilon-P (Millipore, Billerica, MA, USA). The blots were probed with the indicated antibodies, and incubated with horseradish peroxidase-conjugated antibody. Detection of proteins was carried out using ECL advance system (GEHealthcare, Wauwatosa, WI, USA).

Immunoprecipitation

Cells (2×10^6) were lysed in 1 ml of lysis buffer and incubated on ice for 30 min. The total cell lysates were centrifuged at 15,000 rpm for 15 min, at 4 °C and the supernatants were incubated overnight with the first antibody at 4 °C. The complexes were precipitated by adding 30 µl of protein G-agarose beads (GE Healthcare) to the lysate and incubated for 60 min at 4 °C. The beads were centrifuged at 5,000 rpm for 30 s, at 4 °C, and washed five times with ice-cold lysis buffer. The samples were suspended and denatured in SDS sample buffer (50 mM Tris pH 6.8, 2% SDS, 100 mM dithiothreitol, 10% glycerol, 0.01% bromophenol blue).

Reverse transcription-PCR

Total RNA was isolated using TRIzol (Invitrogen). Reverse transcription-PCR (RT-PCR) was performed with total RNA which was reverse transcribed with a cDNA synthesis kit (Invitrogen) with random hexamers. PCR was performed with Takara Taq polymerase (Takara BIO). PCR primer sets were as follows:

CD26 (5′-CGGTCCTGGTCTGCCCCTCTA-3′ and 5′-CGCCACGGCTATTCCACACTT-3′)

CD9 (5′-CCGGTCAAAGGAGGCACCAAG-3′ and 5′-GATAAACTGTTCCACGCCCCC-3′)

GAPDH (5′-ACCACAGTCCATGCCATCAC-3′ and 5′-TCCACCACCCTGTTGCTGTA-3′)

Boyden chamber-based cell invasion and migration assay

For Boyden chamber-based cell invasion assay, tumor cells (0.5×10^4) suspended in 0.5 ml of RPMI-1640 containing 0.1% FCS were plated on Matrigel-coated 8-µm pore diameter polypropylene filter inserts in the Boyden chamber (BD Biosciences). Cells were allowed to migrate for 24 h toward 1 ml of RPMI-1640 containing 10% FCS as chemoattractant. Cells remaining in the insert were removed with a cotton swab, and the cells which attached to the bottom of the filter were stained with Diff-Quick-Staining kit (Sysmex, Kobe, Japan) and counted under optical microscope. At least five fields were counted in each experiment. For assays in the presence of antibodies, cells were pretreated with antibody at the indicated concentration for 15 min at room temperature. For Boyden chamber-based cell motility assay, uncoated inserts (8-µm pore diameter) was used.

MTT proliferation assay

An MTT proliferation assay was performed using TetraColor-ONE system (SeikagakuBioscience, Tokyo, Japan). Cells (2.2×10^3) were plated on a 96 well culture plate in RPMI 1640 containing 10% FCS. Cells were cultured and MTT proliferation assay was performed at indicated times.

In vivo xenograft study

All experiments using mice were approved by and carried out following the guidelines of the Institute Animal Care and Use Committee of the University of Tokyo (Tokyo, Japan). Female SCID mice (5–6 weeks age) were purchased from Charles River (Yokohama, Japan). Mice were anesthetized with ether and subjected to direct s.c. inoculation of mesothelioma cells (5×10^5 per mouse) into the dorsal region. The mice were sacrificed at day 14 after tumor cell implantation and tumors were sampled. Details of animal studies are presented in Checklist S1.

Statistical analysis

The data are shown as the mean ± SE. The statistical significance of differences was evaluated by two-tailed *t*-test, and P values<0.05 was considered significant.

Results

Association of CD26 and CD9 in malignant mesothelioma cell lines

We recently reported that CD26 and CD9 are cancer stem cell markers of malignant mesothelioma [22,23]. Since CD26 and CD9 have been reported to be associated with specific molecules [4,24], we attempted to determine the relationship between CD26 and CD9 in malignant mesothelioma cell lines. We used the mesothelioma cell line ACC-MESO1 (MESO1) cells which

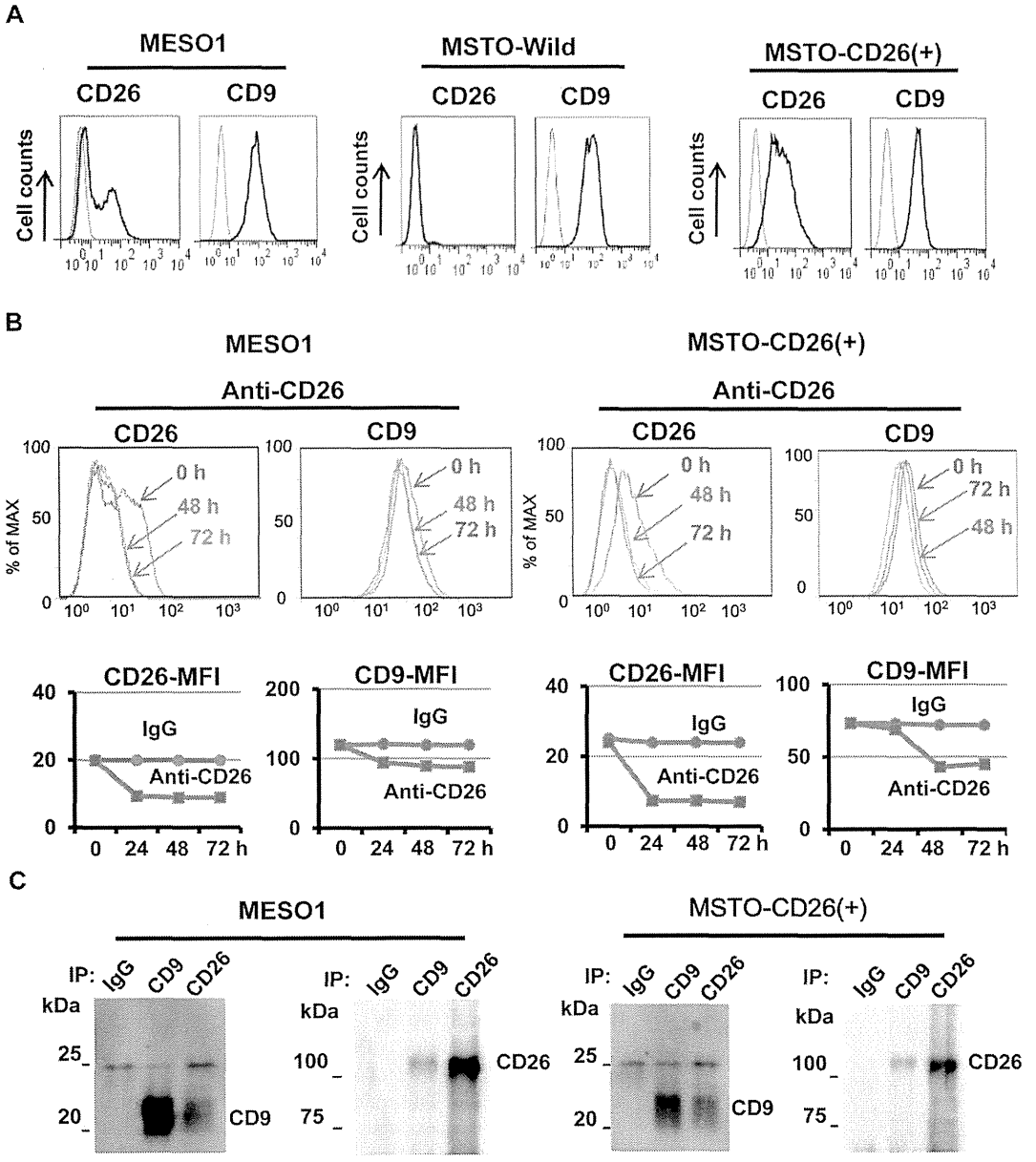

Figure 1. CD26 associates with CD9. (A). Flow cytometric analysis of CD26 and CD9 expression on MESO1, MSTO-Wild or MSTO-CD26 (+) cells. (B). MESO1 or MSTO-CD26 (+) cells were incubated up to 72 h at 37 °C with either control IgG (10 μg/ml) or humanized anti-CD26 mAb (10 μg/ml). These cells were stained with anti-CD26-FITC (5K76) or with anti-CD9-FITC, and subjected to flow cytometry. Intensity of modulation was indicated by mean fluorescence intensity (MFI). (C). MESO1 or MSTO-CD26 (+) cells were subjected to immunoprecipitation with control IgG, humanized anti-CD26 mAb, and anti-CD9 mAb (5H9). Immunoblot was conducted with anti-CD26 polyclonal antibody, and anti-CD9 mAb (5H9). These results were also confirmed by 5 separate experiments.
doi:10.1371/journal.pone.0086671.g001

naturally express CD26, MSTO-211H cells which do not express CD26 (MSTO-Wild), and CD26 transfectant of MSTO-211H cells (designated as MSTO-CD26 (+) cells) (Figure 1A).

We first analyzed antigenic modulation induced by the addition of anti-CD26 mAbin these mesothelioma cells as described previously [29]. As shown in Figure 1B, treatment with anti-CD26 mAb caused modulation of CD26 in MESO1 cells, as well as co-modulation of CD9. Addition of anti-CD26 mAb also caused co-modulation of CD9 and CD26 following 48 to 72 h of incubation in the CD26-transfectant MSTO- CD26 (+) cells (Figure 1B). Immunoprecipitation experiments showed that CD26 and CD9 co-precipitated in MESO1 cells and MSTO-CD26 (+) cells (Figure 1C). These results therefore suggest that CD26 and CD9 have physical and potentially functional association.

The inverse correlation between CD26 and CD9 expression

In order to understand the nature of the association between CD26 and CD9, we performed microarray analysis of CD26-depleted and CD26 over-expressed mesothelioma cells. Interestingly, CD26 depletion augmented CD9, while CD26 overexpression down-regulated CD9. The expression of other tetraspanins such as TSPAN3-5, and CD63 exhibited similar behavior as CD9,

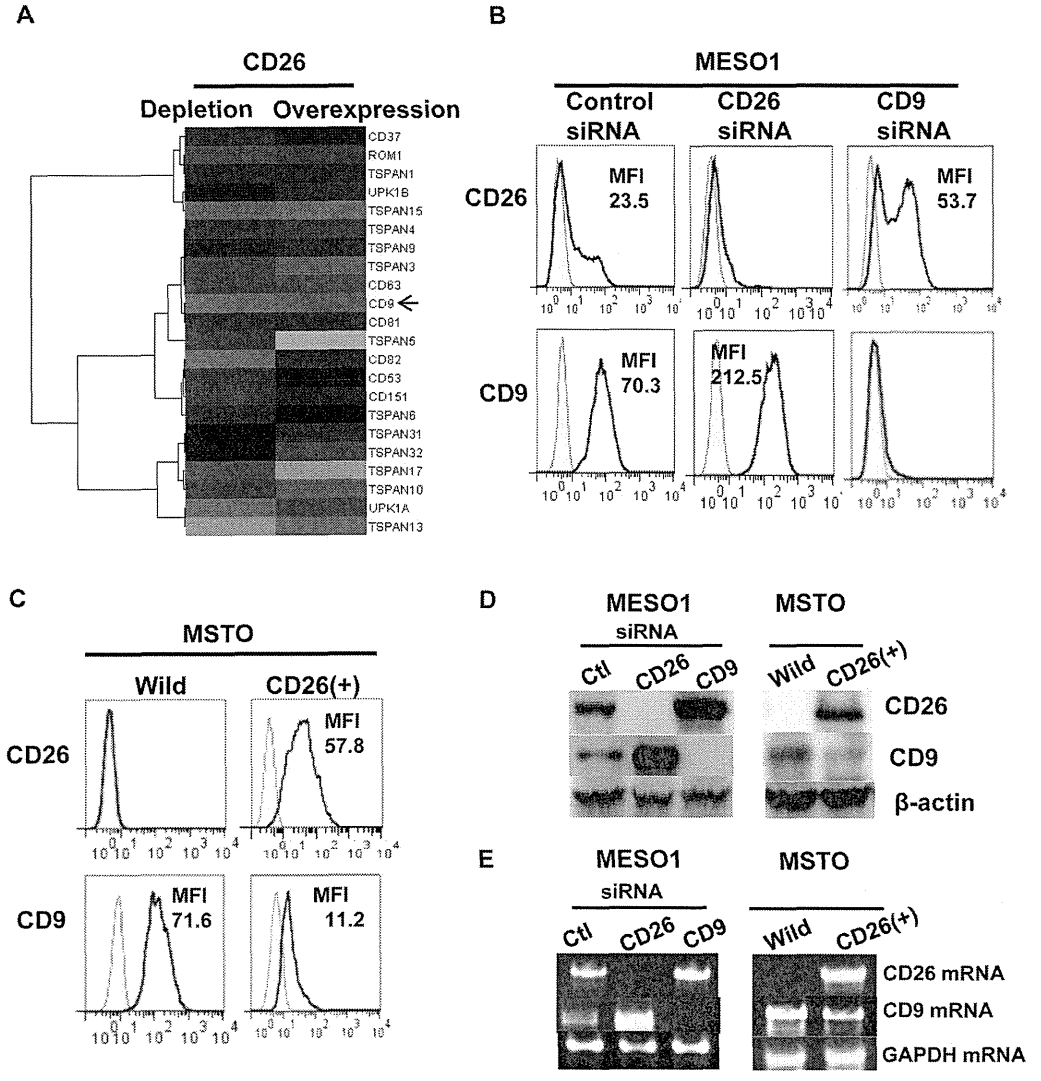

Figure 2. CD26 associates with CD9 in an inverse manner. (A). Heat map representing color-coded expression levels of differentially expressed genes. CD26/Depletion: control siRNA- and CD26 siRNA-transfectedMESO1. CD26/Over expression: MSTO-Wild and MSTO-CD26 (+) cells. Upregulated (red) or downregulated (green). (B and C). MESO1 transfectants of control siRNA, CD26 siRNA, and CD9 siRNA, or MSTO-Wild and MSTO-CD26 (+) cells were stained with anti-CD26-FITC or anti-CD9-FITC and subjected to flow cytometry. (D). MESO1 transfectants with control siRNA, CD26 siRNA, and CD9 siRNA, or MSTO-Wild and MSTO-CD26 (+) cells were lysed and probed with anti-CD26 polyclonal antibody, anti-CD9 mAb (5H9) and anti-β-actin polyclonal antibody. (E). RT-PCR was carried out for analysis of CD26 and CD9 gene expressions on MESO1 transfectants with controlsiRNA, CD26siRNA, and CD9siRNA, or on MSTO-Wild and MSTO-CD26 (+) cells. GAPDH amplification was used as internal control. These results were also confirmed by 5 separate experiments.
doi:10.1371/journal.pone.0086671.g002

whereas that of TSPAN15 and ROM1 displayed the opposite behavior (Figure 2A).

Since microarray analysis indicated that the expression level of CD26 and CD9 was inversely correlated, we examined the effect of CD26 depletion on CD9, and that of CD9 depletion on CD26 expression. Flow cytometric analysis revealed that depletion of CD26 by CD26 siRNA-1 augmented CD9 surface expression, while depletion of CD9 by CD9 siRNA-1 augmented that of CD26 (Figure 2B). Since similar results were obtained using other set of siRNAs for CD26 or CD9 which were designed to target different sites of the gene (data not shown), CD26 siRNA-1 and CD9 siRNA-1 were used for further study.

We next examined the effect of CD26 overexpression on CD9 expression. Flow cytometric analysis showed that CD26-overexpression down-regulated CD9 in MSTO-CD26 (+) cells (Figure 2C). Immunoblotting analysis also confirmed that the protein level of CD9 was elevated after depletion of CD26 mRNA, and that the level of CD26 protein was elevated after depletion of CD9 mRNA in MESO1 cells (Figure 2D). Furthermore, overexpression of CD26 resulted in down-regulation of CD9 (Figure 2D).

RT-PCR analysis confirmed that depletion of CD26 mRNA augmented CD9 gene expression, while CD9 depletion augmented CD26 gene expression in MESO1 cells (Figure 2E). Moreover, RT-PCR analysis confirmed that overexpression of CD26 reduced CD9 gene expression in MSTO-CD26 (+) cells (Figure 2E).

These results indicate that CD26 functionally associates with CD9 in an inverse manner, and that this association may be regulated at the transcriptional level.

An inverse relationship between CD26 and CD9 was also demonstrated in experiments involving CD26 and CD9 shRNAs. In MESO1 cells transduced with CD26 shRNA-1 or CD9 shRNA-1, an inverse correlation between CD26 and CD9 expression was confirmed (Figure S1A), and similar results were also obtained with CD26 shRNA-2 or CD9 shRNA-2 (data not shown). Similar results were also seen in the mesothelioma cell line NCI-H2452 transduced with CD26 or CD9 siRNA (Figure S1B).

CD26 potentiates tumor cell invasion

We next examined the role of CD26 and CD9 association in cellular biology. While flow cytometric analysis showed that MESO1 cells were composed of $CD26^-CD9^-$, $CD26^-CD9^+$, $CD26^+CD9^+$, and $CD26^+CD9^-$ populations (Figure 3A), CD9 expression on $CD26^+CD9^+$ cell surface was lower than on $CD26^-CD9^+$ cells (Figure 3A). Sorting of $CD26^-CD9^+$ cells and $CD26^+CD9^+$ cells by FACS also showed that surface expression of CD9 on $CD26^+CD9^+$ cells was lower than that on $CD26^-CD9^+$ cells (Figure 3B). Immunoprecipitation experiments showed that CD26 co-precipitated with CD9 in $CD26^+CD9^+$ cells (Figure 3B). Therefore, relatively low expression of CD9 on $CD26^+CD9^+$ cells may reflect the inverse relationship between CD9 and CD26 expression in $CD26^+CD9^+$ cells.

Since invasion is an important aspect of malignancy, we compared invasive potential of $CD26^-CD9^+$ cells and $CD26^+CD9^+$ cells using the Boyden chamber-based cell invasion assay. As shown in Figure 3C, markedly higher invasive potential was observed in $CD26^+CD9^+$ cells in sharp contrast to that of $CD26^-CD9^+$ cells.

We next examined invasive potential of $CD26^+CD9^+$ and $CD26^+CD9^-$ cells (Figure 3D). $CD26^+CD9^+$ and $CD26^+CD9^-$ cells were sorted and invasiveness was determined by the same assay (Figure 3E). $CD26^+CD9^-$ cells showed higher invasion activity than that of $CD26^+CD9^+$ cells, suggesting that CD9 may suppress tumor cell invasion. Previous work involving proteomic analysis of human colon cancer cells by LC-MS/MS identified CD26 as one of the CD9-associated proteins in metastatic cells, but not in the primary tumor cells [30]. Although the exact nature of the CD26 and CD9 association was not elucidated in the report, our current data clearly demonstrate that $CD26^+CD9^+$ cells exhibit higher invasive activity than $CD26^-CD9^+$ cells, suggesting that CD26 may potentiate tumor cell invasiveness.

CD9 regulates CD26-mediated tumor cell invasive potential

With our previous data suggesting that CD26 potentiates tumor cell invasiveness, we further evaluated the effect of overexpression

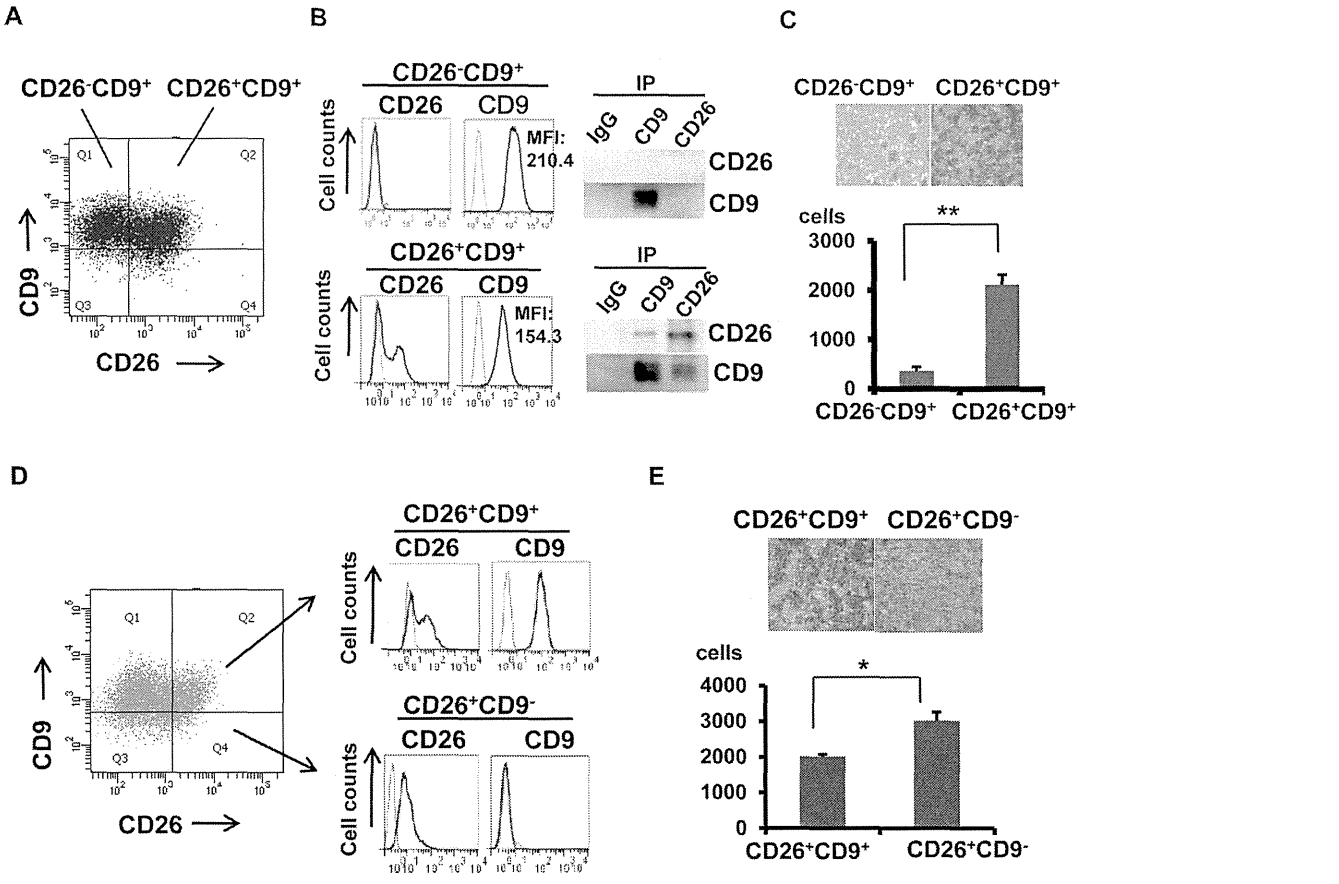

Figure 3. CD26 potentiates tumor cell invasion. (A). Flow cytometric analysis of CD26 and CD9 expressions in MESO1. (B). Sorting of $CD26^-CD9^+$ cells and $CD26^+CD9^+$ cells, and immunoprecipitation was performed with humanized anti-CD26 mAb and anti-CD9 mAb (5H9), then probed with anti-CD26 polyclonal antibody and anti-CD9 mAb (5H9). (C and E).Tumor cell invasion was measured with the Boyden chamber-based cell invasion assay for 24 h. Number of invaded cells was represented as means ± SE (n = 5).*$p<0.01$, **$p<0.001$. (D). Flow cytometric analysis of CD26 and CD9 expressions in MESO1 and sorting of $CD26^+CD9^+$ cells and $CD26^+CD9^-$ cells. These results were also confirmed by 3 separate experiments.

doi:10.1371/journal.pone.0086671.g003

and gene depletion of CD26 on invasiveness and motility of MSTO-CD26(+) and MESO1 cells. As shown in Figure 4A, only a small number of MSTO-Wild cells invaded as compared to a markedly greater number of MSTO-CD26 (+) cells. MESO1 cells which endogenously express CD26 also showed higher level of invasiveness than MSTO-Wild cells (Figure 4A). Meanwhile, this high level of invasiveness was reduced following gene knockdown of CD26 with siRNA (Figure 4B). Similar results were obtained with the cell migration assay (Figure S2A and S2B). These results indicate that CD26 may confer greater tumor cell invasiveness and motility. On the other hand, down-regulation of CD9 by siRNA augmented invasion and migration of MSTO-CD26 (+) and MESO1 cells, but not MSTO-Wild cells (Figure 4C and Figure S2C). In view of previous data suggesting CD9 involvement in suppressing tumor metastasis [17], CD26 ability to promote tumor cell invasion and migration may be influenced by the anti-metastatic activity of CD9. Anti-CD9 mAb treatment consistently enhanced invasiveness and motility of MSTO-CD26 (+) and MESO1 cells, but not MSTO-Wild cells (Figure 4D and Figure S2D). Furthermore, overexpression of CD9 on the CD26-positive mesothelioma cell line NCI-H226 decreased CD26 expression and suppressed invasion (Figure 4E).

Taken together, these results suggest that CD9 regulates migration and invasion of CD26-positive cells by its inhibitory effect on CD26-mediated invasiveness.

CD26 potentiates invasiveness through its association with α5β1 integrin

We next investigated the molecular mechanism involved in CD26 ability to enhance invasiveness of mesothelioma cells. Multiple reports demonstrated that β1 integrins have key roles in cancer metastasis and invasion [31]. Among α1 to α6 integrins, α5 and α6 integrins were detected on the surface of MESO1 and MSTO- CD26 (+) cells. Meanwhile, treatment with anti-CD26 mAb led to co-modulation of α5β1, but not α6β1 integrin, in MESO1 and MSTO-CD26 (+) cells (data not shown).

Additional analysis of the interaction between α5β1 integrin and CD26 showed that transfection of CD26 cDNA into MSTO-Wild cells increased the level of α5β1 expression (Figure 5A). Immunoprecipitation analysis indicated that α5β1 integrin co-precipitated with CD26, but not with CD9 in MESO1 and MSTO-CD26 (+) cells (Figure 5B). These data therefore suggest that CD26 associates with α5β1 integrin in mesothelioma cells.

We next studied the effect of antibodies against α5 and β1 on invasiveness according to previously described methods [26]. Treatment with anti-integrin α5 or β1 mAb inhibited tumor cell invasion and migration of MESO1 and MSTO-CD26 (+) cells (Figure 5C and 5D). Therefore the present results indicate that α5β1 integrin may play an important role in CD26-mediated promotion of migration and invasion in mesothelioma cells.

Down-regulation of CD9 enhances invasiveness through its inverse relationship with CD26

We next evaluated the effects of CD9 down-regulation on invasiveness of CD26-positive cells. SiRNA-mediated CD26 depletion of CD26-positive cells led to reduced α5β1 integrin level as detected by immunoblotting (Figure 6A). These results confirm that CD26 potentiates tumor cell invasiveness through its regulation of α5β1 integrin. On the other hand, siRNA-mediated depletion of CD9 augmented the expression of CD26 and α5β1 integrin, as detected by immunoblotting (Figure 6B). Since CD9 itself does not associate with α5 integrin (Figure 5B), it is plausible that down-regulation or perturbation of CD9 may augment CD26 expression in an inverse manner, and the resultant increased level of the CD26-α5β1 complex likely contributes to enhanced invasive potential. Since CD9 overexpression led to decreased CD26 expression and suppression of tumor cell invasion (Figure 4E), we next determined the effect of CD9 overexpression on α5β1 integrin expression. On CD9-overexpressed NCI-H226 cells, the expression of α5β1 integrin was reduced together with that of CD26 (data not shown). Therefore, the opposing effect of CD9 and CD26 on migration and invasive potential is mediated at least partly through their effect on α5β1 integrin expression.

We previously demonstrated that Crk-associated substrate lymphocyte type (Cas-L)/human enhancer of filamentation 1 (HEF1)/neural precursor cell expressed, developmentally down-regulated 9 (NEDD9) mediates cell signaling through β1 integrins [32–34], and that Cas-L promotes metastasis of non-small cell lung cancer cells [35]. We therefore examined the possible involvement of Cas-L in CD26-mediated mesothelioma cell invasiveness. Immunoprecipitation experiments indicated that β1 associates with focal adhesion kinase (FAK), and FAK with Cas-L in MESO1 and MSTO-CD26 (+) cells (Figure 6C). CD26 depletion by siRNA resulted in decreased expression of FAK and Cas-L, while CD9 depletion augmented FAK and Cas-L level in MESO1 and MSTO-CD26 (+) cells (Figure 6D). These results hence suggest the involvement of FAK and Cas-L in CD26-mediated invasiveness.

Since CD9 depletion led to increased CD26 expression (Figure 2B, Figure 6B, and Figure S1) and promoted invasiveness and motility (Figure 4C and Figure S2C), we evaluated the effect of CD9 depletion on tyrosine phosphorylation levels of FAK and Cas-L. As shown in Figure 6E, CD9 depletion led to increased FAK and Cas-L tyrosine phosphorylation in mesothelioma cells, indicating that CD26 and CD9 may regulate the overall protein level and tyrosine-phosphorylation of β1 integrin-related signaling molecules as well as the expression of α5β1 integrin.

Combined treatment with anti-CD26 mAb and anti-CD9 mAb on tumorigenesis

Our present study indicated that blocking of CD26 expression by gene-depletion inhibited tumor cell invasiveness. Since CD26 interacts with CD9 in an inverse correlation, it is plausible that combined blocking of both CD26 and CD9 may effectively inhibit tumor cell invasiveness. We then examined the effect of combined blocking of CD26 and CD9 with their respective antibodies. In MSTO-CD26(+) cells, anti-CD26 mAb inhibited tumor cell invasiveness. As shown in Figure 4D, anti-CD9 mAb treatment enhanced invasiveness (Figure 7A). However, combined treatment with anti-CD26 mAb and anti-CD9 mAb markedly inhibited invasiveness (Figure 7A). Similar results were obtained in MESO1 cells (Figure 7A).

We next examined the effects of combined blocking of CD26 and CD9 on tumor cell proliferation. CD26-depletion with shRNA inhibited in vitro tumor cell growth of MESO1 cells (Figure 7B). In contrast to the enhanced effects on invasiveness by CD9-depletion, gene-depletion of CD9 inhibited tumor growth (Figure 7B). Furthermore, combined depletion of both CD26 and CD9 effectively inhibited in vitro tumor growth (Figure 7B). Similarly, blocking of CD26 or CD9 by antibodies inhibited in vitro tumor growth in MSTO-CD26(+) and MESO1 cells (Figure 7C). Moreover, combined treatment with anti-CD26 mAb and anti-CD9 mAb resulted in enhanced inhibition of tumor growth in these cell lines (Figure 7C). In mouse xenograft study, depletion of CD26 or CD9 by shRNA inhibited in vivo tumor growth (Figure 7D), and combined depletion of CD26 and CD9 caused prominent suppression of tumor growth in vivo (Figure 7D).

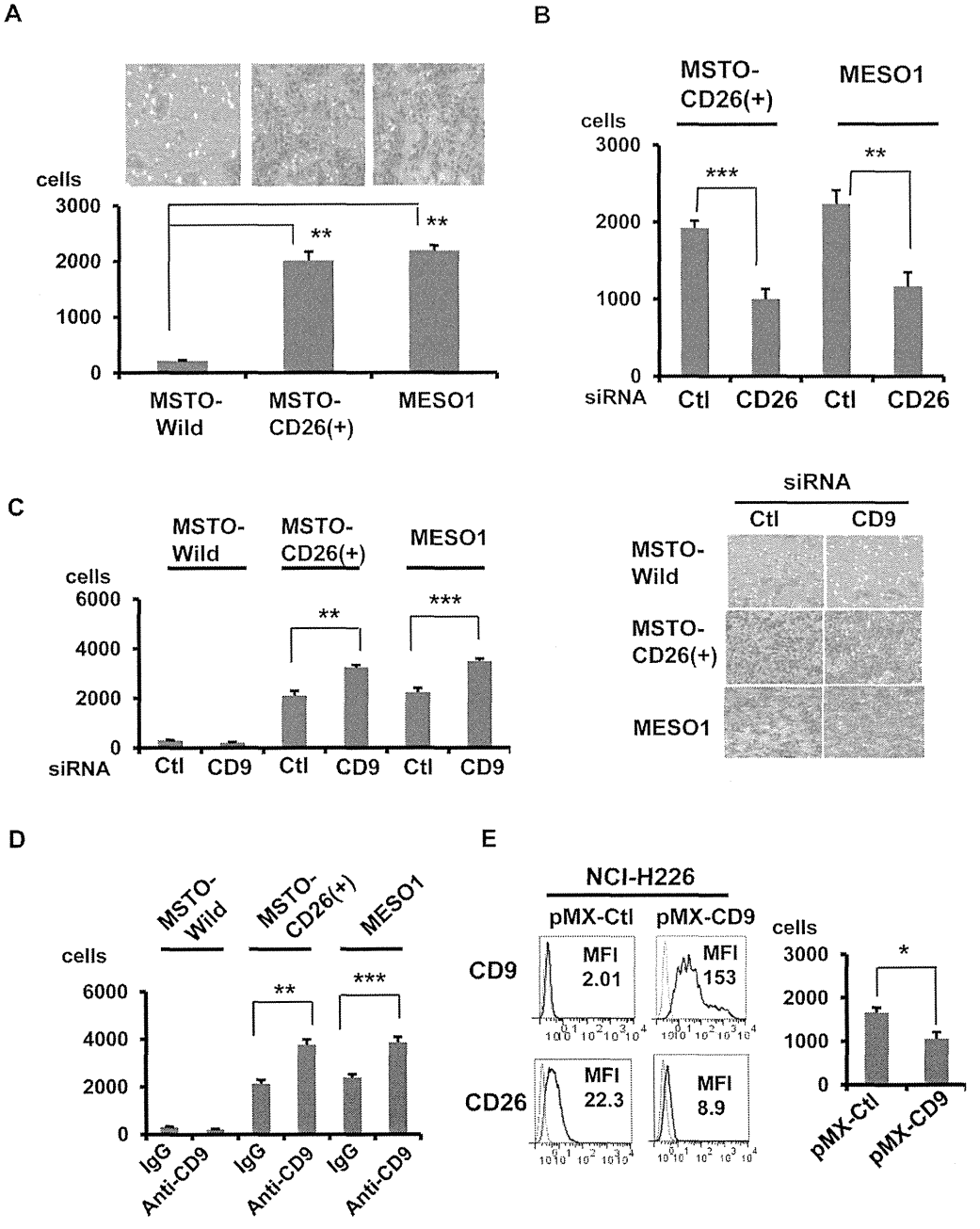

Figure 4. CD9 negatively regulates CD26-mediated invasion. (A-E).Cells were analyzed by the cell invasion assay for 24 h. Number of invaded cells were represented as means ± SE (n = 5). (A). MSTO-Wild,MSTO-CD26 (+), and MESO1 cells. Invaded cells stained are shown in the top panel. **p<0.005. (B). MSTO-CD26 (+) or MESO1 cells transfected with controlsiRNA or CD26siRNA. **p<0.005, ***p<0.001. (C). MSTO-Wild,MSTO-CD26 (+), and MESO1 cells transfected with control-siRNA or CD9siRNA. Invaded cells stained are shown in the right panel. **p<0.005, ***p<0.001. (D). MSTO-Wild, MSTO-CD26 (+), and MESO1 cells treated with control IgG or anti-CD9 mAb (10 μg/ml).**p<0.005, ***p<0.001. (E). NCI-H226 was transfected with pMX vector control or pMX-CD9. After staining with CD26-FITC and CD9-FITC, cells were subjected to flow cytometry.Boyden chamber-based cell invasion assay was performed with NCI-H226 transfected with pMX vector control or pMX-CD9 for 24 h. Number of invaded cells/well was represented as means ± SE (n = 5).*p<0.05.
doi:10.1371/journal.pone.0086671.g004

Similarly, anti-CD26 mAb or anti-CD9 mAb inhibited tumor growth in vivo. Furthermore, combined treatment with anti-CD26 mAb and anti-CD9 mAb resulted in marked inhibition of tumor growth in vivo. Therefore, combined blockade of both CD26 and CD9 might be a potential therapeutic approach for malignant mesothelioma.

Discussion

In the present study, we propose a novel molecular mechanism that involves the reciprocal interaction of CD26 and CD9. We first demonstrated antibody-induced co-modulation and co-precipitation of CD9 and CD26. At the transcriptional level, expression of CD9 and CD26 mRNAs was regulated in an inverse manner. Meanwhile, these molecules exhibited opposite effects on invasion

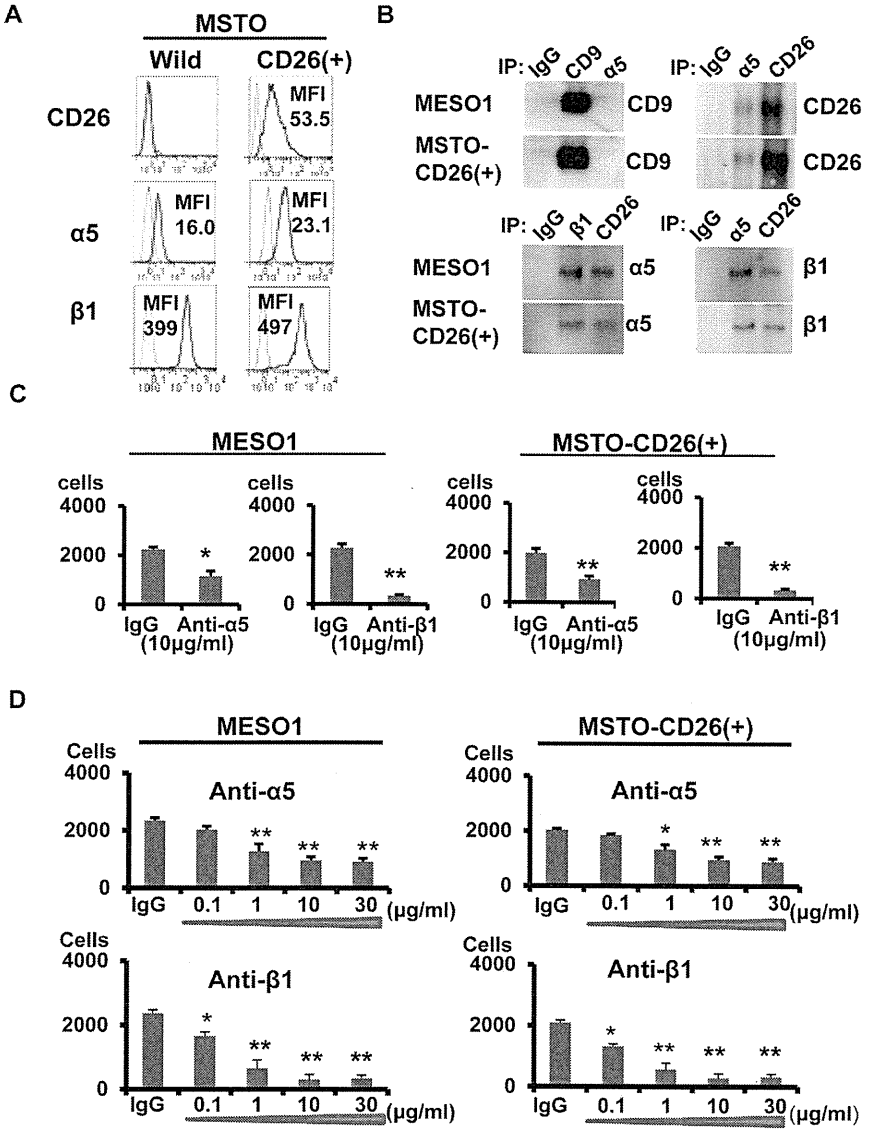

Figure 5. CD26 potentiates invasiveness through α5β1 integrin. (A).MSTO-Wild, MSTO-CD26 (+) cells were subjected to flow cytometry for CD26, α5, and β1. (B). MESO1 and MSTO-CD26 (+) cells were subjected to immunoprecipitation with control IgG, humanized anti-CD26 mAb, anti-CD9 mAb (5H9), anti-α5 mAb (2H6), or anti-β1 mAb (4B4). The immunoblot was probed with anti-CD26 polyclonal antibody, anti-CD9 mAb (5H9), anti-α5 mAb (2H6), or anti-β1 mAb (4B4). (C). Boyden chamber-based cell invasion assay of MESO1 and MSTO-CD26 (+) cells treated with anti-α5, and β1 antibodies for 24 h. (n = 5). *$p<0.01$, **$p<0.005$. (D).The cell migration assay of MESO1 and MSTO-CD26 (+) cells treated with anti-α5, and β1 antibodies.(n = 5). *$p<0.05$, **$p<0.01$.
doi:10.1371/journal.pone.0086671.g005

and migration of mesothelioma cells, with CD26 having an enhancing effect and CD9 showing a suppressing effect. These contrasting effects of CD9 and CD26 were further elucidated by gene knockdown and gene transfer experiments. Furthermore, we demonstrated co-precipitation of CD26 and α5β1 integrin adhesion receptor, which partially explains the pro-metastatic behaviors of $CD26^+$ tumor cells. Finally, perturbation of CD26 or CD9 expression resulted in changes of the overall protein and tyrosine-phosphorylation levels of FAK and Cas-L, the β1 integrin-mediated signaling molecules involved in cell adhesion and migration.

Tetraspanins form complexes by interacting with other tetraspanins as a homodimer or a heterodimer and with other classes of molecular species that are required for their biological function [24]. Molecular compensation is one of the characteristics of tetraspanins. Depletion of individual tetraspanin which forms embryonic synapse in Drosophila results in minor defects in development due to the overlapping expression of tetraspanins with similar functions, which compensates for the absence of another tetraspanin [36]. Compared with single knockdown of these tetraspanins, depletion of two or three tetraspanins markedly decreased cancer cell invasion, due to the overlapping contributions of these tetraspanins [37]. These molecular compensations are supported by overlapping expression of tetraspanins with similar functions. In contrast to the reported molecular compensations based on overlapping expressions of tetraspanins, our current work demonstrates an association between tetraspanin and non-tetraspanin molecules to regulate their expressions in an inverse manner. This kind of association has been recently reported in the case of CD9 and CD9P-1, in which the expression